Chapter 6

PERFORMANCE IMPROVEMENT FROM OPTICAL MODULATION FORMATS IN PRACTICAL SYSTEMS

In the previous chapter (Chapter 5), the system performance in terms of normalized system parameters was investigated. It was shown that system performance can be improved by employing appropriate optical modulation formats instead of simple RZ format. However, the optical fiber used in that investigation is assumed to be linear and lossless, which differs from an actual optical fiber. In addition, there are several types of optical fibers, each designed for specific system configurations. When the devices used in a system are considered, some introduce noise into the system, which impairs the system performance. The transmitted data may not be recovered correctly at the receiver in the presence of noise. Therefore, the performance measure used in the investigations in this chapter is no longer the eye opening, but the probability of bit error P_e. The probability of bit error is a more meaningful performance measure than the eye opening when noise is present. It should be noted, however, that the probability of bit error is still derived from the eye opening, which will be discussed later in this chapter.

The main objective of this chapter is to investigate the performance improvements obtained from different optical modulation formats in practical system configurations. Currently, the trend in the bit rate per channel is moving from 10 Gb/s to 40 Gb/s to maximize the aggregated bit rate per fiber; hence, the bit rate considered in the investigations is 40 Gb/s. As discussed in Chapter 2 and Chapter 3, the interchannel impairments can be made negligible with proper system design by means of appropriate channel spacing, transmission fiber configuration, and optical modulation format. In that case, the intrachannel impairments are the major obstacles in maximizing the system performance. Thus, our main focus is on the improvement obtained from different optical modulation formats in combating the intrachannel impairments. That is, only a single-channel is considered.

Recall from Chapter 2, the transmission fibers can be divided into three categories based on their local dispersion: small, moderate and large local dispersion. In this chapter, single-span systems employing optical fibers having small, moderate, and large dispersions are investigated. Note that at the bit rate as high as 40 Gb/s, the transmission fibers having moderate and large dispersions require dispersion compensation due to large accumulated dispersion. In addition, multiple-span dispersion-managed systems employing in-line optical amplifiers to extend the transmission distance are also investigated. This chapter is organized as follow. The mathematical model of the receiver is discussed in the first section. The mathematical expressions used to evaluate the system performance in terms of the bit error rate are provided in Section 6.2. In Section 6.3 is the discussion of system performance for a single-span system employing an optical fiber having small local dispersion. The optical modulation formats considered are sinusoidal alternating phase modulation (APM), sinusoidal same phase modulation (SaPM), square wave phase modulation (SWM), continuous-wave square-wave (CWSW), optical duobinary, alternate mark inversion (AMI), and a conventional RZ format with no PM (No PM). It is found that CWSW and AMI provide better performance improvement than the other modulation formats. Therefore, the remaining sections are focused on the performance improvement obtained from CWSW and AMI while no PM is still considered for reference purposes. In Section 6.4 the discussion of the performance improvement in a single-span system employing an optical fiber having small local dispersion is continued; however, an optical preamplifier is employed in the receiver in this case in order to extend the transmission distance. The studies of system performance in a single-span dispersion-managed system are provided in Section 6.5. The transmission fibers investigated are those having moderate and large local dispersions. The transmission distance can be increased significantly by employing an in-line optical amplifier to periodically boost up the signal power. The investigation of system performance in such a system is in Section 6.6. The effect of the optical filter at the fiber input in the case of CWSW signal is discussed in Section 6.7. The final section of this chapter, Section 6.8, is the summary.

6.1 RECEIVER CIRCUIT STRUCTURE AND MATHEMATICAL MODEL

The main task of the receiver is to convert an optical signal to an electrical signal, which is then amplified, filtered, and sampled. The receiver in general consists of a *pin* photodiode followed by a transimpedance amplifier [139]. (*pin* comes from the fact that the photodiode is a semiconductor device consisting of p and n regions with a lightly doped intrinsic (i) region in the middle between those two regions [58].) The electrical output signal from the amplifier is then fed to the decision circuit. The signal is sampled and compared with a threshold to decide whether bit 0 or bit 1 was transmitted. Shown in Fig. 6.1 is the equivalent schematic diagram of the receiver. The amplifier is modeled as a lowpass filter with a thermal noise source $i_{th}(\tau_n)$ at its input. The output photocurrent from the photodiode caused by the incident optical signal is given by

$$i_{ph}(\tau_n) = \frac{\mathcal{R}}{2}\left|q_{out}(\tau_n)\right|^2 \tag{6.1}$$

where $q_{out}(\tau_n)$ is the baseband complex envelope of the incident electric field, and $\mathcal{R}$ is the responsivity of the photodiode. The factor of $1/2$ in (6.1) comes from the fact that the power of the incident optical signal is half the power of the corresponding baseband complex envelope. $\mathcal{R}$ can be related to the quantum efficiency η of the photodiode by

$$\begin{aligned}\mathcal{R} &= \eta\frac{q_e\lambda_0}{hc} \\ &= \eta\frac{\lambda_0[\mu\text{m}]}{1.24}\end{aligned} \tag{6.2}$$

where q_e is the elementary charge constant, h is Planck's constant, c is the speed of light in vacuum, and λ_0 is the wavelength of the incident optical signal. The quantum efficiency η in (6.2) is the figure of merit that indicates the effectiveness of the photodiode. It is defined as the ratio between the average number of electrons flowing out to the external circuit per unit time and the number of photons incident on the photodiode per unit time; hence, η ranges from 0 to 1. In general, η is less than unity, and its typical value is 0.7 [139].

When a constant optical signal intensity is incident on the photodiode, the generation of the photoelectrons is not deterministic in nature due to the random arrival time of the incident photons. Thus, there is a fluctuation of the photocurrent about its average value at the photodiode output. This fluctuation is known as shot noise. However, the shot noise is negligible compared to the receiver thermal noise when a *pin* photodiode is employed. The receiver thermal noise current $i_{th}(\tau_n)$ referred back to the output of the photodiode is a Gaussian random process having zero mean, whose variance is given by [139]

$$\sigma_{th}^2 = \frac{4kTB_e}{R_e} \tag{6.3}$$

where k is the Boltzmann's constant, T is room temperature, B_e is the equivalent noise bandwidth, and R_e is the effective noise resistance of the amplifier. The equivalent noise bandwidth B_e in (6.3) can be written as a function of amplifier parameters as

$$B_e = \frac{1}{2\pi R_e C_e}. \tag{6.4}$$

where C_e is the effective noise capacitance of the amplifier . For a practical receiver, $C_e \approx 0.1$ pF [139]. By substituting (6.4) into (6.3), σ_{th}^2 becomes

$$\sigma_{th}^2 = 8\pi V_T B_e^2 C_e \tag{6.5}$$

where V_T is the thermal voltage defined as

$$V_T = \frac{kT}{q_e}. \tag{6.6}$$

Note that the thermal voltage given by (6.6) is equal to 0.025 V at the room temperature of 290 K. The variance of the receiver thermal noise given by (6.3) is in fact the variance of the signal when the receiver thermal noise is the dominant noise source. It should be noted at this point that the receiver thermal noise is not the only noise source in a system. For example, if there is an optical preamplifier in the system, the preamplifier itself is an additional noise source, generating amplified spontaneous emission (ASE) noise. All of these lead to the signal fluctuation, which in effect may cause bit errors on recovered data.

6.2 PERFORMANCE MEASURES

In optical fiber communication systems, the fiber chromatic dispersion and nonlinear effects degrade the eye opening (*EOP*). In addition, the accumulated noise at the receiver results in signal fluctuation at the decision time, which can cause errors in the recovered data. When the probability of bit error P_e is very small (e.g. 10^{-9}), the most appropriate way is to determine P_e analytically. In order to do so, the exact probability density functions (pdf) of the signal representing bit 1 and bit 0 at the decision time are required. Unfortunately, this is very difficult to obtain in practice. When the receiver thermal noise is the dominant noise source, those pdf's are close to Gaussian. This is not true for optical amplifier systems because the pdf of the photocurrent due to the ASE noise is not Gaussian [140], [141]. However, a good estimation of P_e can still be achieved with the Gaussian approximation although the exact distributions of the signals are not Gaussian [142], [143].

Let the pdf's of the signal representing bit 1 and bit 0 referred back to the output of the photodiode be p_1 and p_0, respectively. Then, the probability of bit error can be found from

$$P_e = \frac{1}{2}\int_{-\infty}^{I_{th}} p_1(\xi)d\xi + \frac{1}{2}\int_{I_{th}}^{\infty} p_0(\xi)d\xi , \tag{6.7}$$

where I_{th} is the threshold. By differentiating P_e given by (6.7) with respect to I_{th}, and setting the resultant expression to zero, the optimum threshold has to satisfy

$$p_1(I_{th}) = p_0(I_{th}) . \tag{6.8}$$

The receiver decides that bit 1 was transmitted when the photocurrent exceeds I_{th}, and that bit 0 was transmitted when the photocurrent is less than I_{th}. By using the assumptions that both p_1 and p_0 are Gaussian distributed and that both integrals in (6.7) are equal, the probability of bit error is then given by

$$P_e = \frac{1}{2\pi}\int_Q^{\infty} \exp\left(-\frac{\xi^2}{2}\right) d\xi \,, \tag{6.9}$$

where

$$Q = \frac{\mu_1 - \mu_0}{\sigma_1 + \sigma_0}, \tag{6.10}$$

and μ_1 and σ_1 are the average photocurrent and standard deviation for bit 1 referred back to the output of the photodiode, respectively, and μ_0 and σ_0 are the average photocurrent and standard deviation for bit 0 referred to the output of the photodiode, respectively. As seen from (6.10), the advantage of the Gaussian approximation is that the probability of bit error P_e can be approximated from the means (μ_1 and μ_0) and standard deviations (σ_1 and σ_0). It should be noted, however, that the threshold I_{th} predicted by the Gaussian approximation is not at the optimum due to the exact distributions of the signal not being Gaussian, but the Gaussian approximation yields a very close estimation of P_e to the value calculated from the exact signal distributions [142], [143]. In other words, the Gaussian approximation is suitable for predicting P_e, but not the threshold I_{th}.

Similar to Chapter 5, a pseudo random data sequence of length 128 is used in the numerical simulations conducted in this chapter. In order not to overestimate system performance, $\mu_1 - \mu_0$ in (6.10) is replaced by eye opening (EOP), which is defined as the difference between the lowest photocurrent representing bit 1 and the highest photocurrent representing bit 0 at the decision time (at the middle of a bit slot). The eye opening is generally a conservative estimate of $\mu_1 - \mu_0$ when the pattern length is short. Thus, (6.10) is changed to

$$Q = \frac{EOP}{\sigma_1 + \sigma_0}. \tag{6.11}$$

It should be noted that low frequency cut-off effects at the receiver, that would necessitate consideration of longer patterns, are not considered in this dissertation. From the eye diagrams, obtained from numerical simulations without considering the noise in the system, the eye opening (EOP) can be determined, and then the signal fluctuations caused by noise (σ_1 and σ_0) are numerically calculated separately to semi-analytically

determine the system performance by using (6.11). In general, Q is used to represent the system performance instead of P_e. For a probability of bit error P_e of 10^{-9}, the corresponding value of Q is equal to 6 (15.6 dB). Thus, the threshold value of Q is 15.6 dB.

For single-link systems, not employing optical amplifiers, the system block diagram mainly consists of a transmitter, an optical fiber, and a receiver. The noise associated with system components at the transmitter can be safely ignored because the noise at the transmitter is negligible compared with the transmitted signal power. Therefore, the dominant source of signal fluctuation is the thermal noise at the receiver. In this case, (6.11) becomes

$$Q = \frac{EOP}{2\sigma_{th}} \tag{6.12}$$

where σ_{th} can be found from (6.5). It is clearly seen from (6.12) that the estimation of the Q value for single-link systems, without optical amplifiers, is fairly simple. However, when an optical amplifier is utilized in a system to improve the system performance, the amplifier also introduces ASE noise into the system, which makes the calculation of the noise at the receiver more complicated. This is discussed in the next section.

6.2.1 Single-Span Systems with Optical Preamplifier

Since an optical fiber is a dispersive nonlinear channel, the EOP generally degrades with increased transmission distance z. Additionally, fiber loss also decreases the signal power at the receiver. In order to keep Q to an acceptable level at a large transmission distance z, the signal power at the receiver has to be sufficiently large compared to the noise at the receiver. This cannot be accomplished simply by increasing the transmitted signal power, because the nonlinear effects in an optical fiber are proportional to the transmitted signal power. One solution is to employ an optical amplifier as a preamplifier in the receiver. The schematic diagram of an optical preamplifier system is as shown in Fig. 6.2a. The optical preamplifier and the optical filter are placed at the optical fiber output in front of the receiver. Since the optical amplifier is not ideal, there is an amplified spontaneous emission (ASE) noise in the

amplification process, which is similar the thermal noise generated in electronic devices. Therefore, an optical filter is required at the optical preamplifier output in order to limit the ASE noise.

The ASE noise at the output of the optical filter with noise equivalent bandwidth of B_0 can be modeled as a bandpass Gaussian noise process having a bandwidth of B_0 [144]. The ASE noise power in one polarization is given by [144]

$$P_{ASE} = n_{sp} h\nu (G-1) B_0 \tag{6.13}$$

where n_{sp} is the spontaneous emission factor or population-inversion factor, $\nu = c/\lambda_0$ is the operating frequency, and G is the optical preamplifier gain. The value of the spontaneous emission factor n_{sp} is unity when the amplifier achieves complete population inversion; however, n_{sp} is usually greater than unity in practice, and two is the typical value. When the amplifier gain G is sufficiently large, the amplifier noise figure F_n as a function of the spontaneous emission factor n_{sp} is simply given by $F_n \approx 2n_{sp}$.

When the optical preamplifier is assumed to have flat gain of G over the frequency range occupied by the signal, the photocurrent at the output of the photodiode under the presence of ASE noise is given by

$$i_{ph}(\tau_n) = \frac{\mathcal{R}}{2}\left|\sqrt{G}\cdot q_{ftr,out}(\tau_n) + x(\tau_n) - jy(\tau_n)\right|^2 + \frac{\mathsf{R}}{2}\left|+\tilde{x}(\tau_n) - j\tilde{y}(\tau_n)\right|^2 \tag{6.14}$$

where $q_{ftr,out}(\tau_n)$ is the baseband complex envelope of the electric field at the optical filter output when the input is the electric field output from the optical fiber $q_{out}(\tau_n)$. In (6.14), the in-phase and quadrature components of the ASE noise having the same polarization as the intended signal $q_{ftr,out}(\tau_n)$ are denoted by $x(\tau_n)$ and $y(\tau_n)$, respectively, while the orthogonal polarization components are denoted by $\tilde{x}(\tau_n)$ and $\tilde{y}(\tau_n)$. Note that $x(\tau_n)$, $y(\tau_n)$, $\tilde{x}(\tau_n)$, and $\tilde{y}(\tau_n)$ are independent identically distributed baseband Gaussian random processes with zero-mean and bandwidth of $B_0/2$. The variance of each process is equal to σ_x^2, which is the ASE noise power in one polarization and, thus, equal to

$$\sigma_x^2 = n_{sp} h\nu (G-1) B_0 . \tag{6.15}$$

The output photocurrent from the photodiode given by (6.14) can be divided into three parts: the signal photocurrent $i_q(\tau_n)$, the signal-spontaneous photocurrent $i_{q-sp}(\tau_n)$, and the spontaneous-spontaneous photocurrent $i_{sp-sp}(\tau_n)$ [145]. That is, (6.14) can be written as

$$i_{ph}(\tau_n) = i_q(\tau_n) + i_{q-sp}(\tau_n) + i_{sp-sp}(\tau_n). \tag{6.16}$$

where

$$i_q(\tau_n) = \frac{\mathcal{R}G}{2}\left|q_{ftr,out}\right|^2, \tag{6.17}$$

$$i_{q-sp}(\tau_n) = \frac{\mathcal{R}\sqrt{G}}{2}\left[\left(q_{ftr,out} + q^*_{ftr,out}\right)x + j\left(q_{ftr,out} - q^*_{ftr,out}\right)y\right], \tag{6.18}$$

and

$$i_{sp-sp}(\tau_n) = \frac{\mathcal{R}}{2}\left[x^2 + y^2 + \tilde{x}^2 + \tilde{y}^2\right]. \tag{6.19}$$

The first term on the right hand side of (6.16) $i_q(\tau_n)$ is due to the intended signal; hence, it does not give rise to an additional noise at the receiver assuming that the gain of the preamplifier is sufficiently large that shot noise is negligible. The terms on the right hand side of (6.16) that contribute additional noise at the receiver are the second term and the last term. The noises caused by $i_{q-sp}(\tau_n)$ and $i_{sp-sp}(\tau_n)$ are usually called the signal-spontaneous beat noise and spontaneous-spontaneous beat noise, respectively. Since x and y have zero mean, the average value of $i_{q-sp}(\tau_n)$ is zero. On the other hand, the average value of $i_{sp-sp}(\tau_n)$ is given by

$$E[i_{sp-sp}(\tau_n)] = 2\mathcal{R}\sigma_x^2, \tag{6.20}$$

where $E[...]$ is the expected-value operation. It should be noted that the average value of $i_{sp-sp}(\tau_n)$ does not affect the eye opening EOP because $i_{sp-sp}(\tau_n)$ is independent of the intended signal.

In order to find σ_1 and σ_0, the variances of signal-spontaneous beat noise and spontaneous-spontaneous beat noise have to be evaluated. By using (6.18), the variance of the signal-spontaneous beat noise is given by

$$\mathrm{var}\left[i_{q-sp}(\tau_n)\right] = \mathcal{R}^2 G\sigma_x^2 E\left[\left|q_{ftr,out}(\tau_n)\right|^2\right], \tag{6.21}$$

where $\mathrm{var}[\xi] = E[\xi^2] - E^2[\xi]$ is the variance of a random variable ξ. Up to this point the effect of the electrical lowpass filter on the variance of the signal-spontaneous beat noise $i_{q-sp}(\tau_n)$ given by (6.21) has not been taken into account yet. Due to the beating between the signal and the ASE noise, the bandwidth of the signal-spontaneous beat noise $i_{q-sp}(\tau_n)$ is larger than the baseband bandwidth of the ASE noise, which is equal to $B_0/2$. By using the assumption that the bandwidth of $i_{q-sp}(\tau_n)$ is approximately equal to $B_e + B_0/2$, the variance of the signal-spontaneous beat noise referred back to the photodiode output can be written as

$$\sigma_{q-sp}^2 = \mathcal{R}^2 G\sigma_x^2 E\left[\left|q_{ftr,out}(\tau_n)\right|^2\right]\frac{B_e}{(B_e + B_0/2)}, \tag{6.22}$$

where the factor of $B_e/(B_e + B_0/2)$ represents the effect of the electrical filter on the signal-spontaneous beat noise. It is clearly seen from (6.22) that σ_{q-sp}^2 is a function of $q_{ftr,out}(\tau_n)$; therefore, the variances of signal-spontaneous beat noise for bit 1 and bit 0 are not identical. Since $q_{ftr,out}(\tau_n)$ is the baseband complex envelope of the actual signal, $E\left[\left|q_{ftr,out}(\tau_n)\right|^2\right]$ in (6.22) can be expressed as a function of the average optical power of $q_{ftr,out}(\tau_n)$ as

$$E\left[\left|q_{ftr,out}(\tau_n)\right|^2\right] = 2P_{r,q} \tag{6.23}$$

where $P_{r,q}$ is the average optical power of $q_{ftr,out}(\tau_n)$ which can be evaluated from

$$P_{r,q} = \lim_{T\to\infty}\frac{1}{T}\int_{-T/2}^{T/2}\frac{1}{2}\left|q_{ftr,out}(\tau)\right|^2 d\tau. \tag{6.24}$$

It should be noted that the average optical power $P_{r,q}$ in (6.24) can also be expressed as

$$P_{r,q} = \frac{P_{r,1} + P_{r,0}}{2}, \tag{6.25}$$

where $P_{r,1}$ and $P_{r,0}$ are the average optical powers of $q_{ftr,out}(\tau_n)$ for bit 1 and bit 0, respectively. Hence, the signal-spontaneous beat noises for bit 1 and bit 0 can be related

to the average optical power of bit 1 and bit 0, respectively. By substituting (6.15), (6.23) and (6.25) into (6.22), σ_{q-sp}^2 becomes

$$\sigma_{q-sp}^2 = \frac{\sigma_{q-sp,1}^2 + \sigma_{q-sp,0}^2}{2} \tag{6.26}$$

where $\sigma_{q-sp,1}^2$ and $\sigma_{q-sp,0}^2$ are the variances of the signal-spontaneous beat noise for bit 1 and bit 0, respectively, and they are given by

$$\sigma_{q-sp,1}^2 = 2\eta^2 q_e \left(\frac{q_e}{h\nu}\right) G(G-1) n_{sp} B_0 P_{r,1} \frac{B_e}{(B_e + B_0/2)}, \tag{6.27}$$

and

$$\sigma_{q-sp,0}^2 = 2\eta^2 q_e \left(\frac{q_e}{h\nu}\right) G(G-1) n_{sp} B_0 P_{r,0} \frac{B_e}{(B_e + B_0/2)}. \tag{6.28}$$

The variances given by (6.27) and (6.28) are in fact the powers of the signal-spontaneous beat noise for bit 1 and bit 0, respectively, that cause additional signal fluctuation at the receiver. It should be noted that the existence of the variance of the signal-spontaneous beat noise for bit 0 is due to ISI in empty bit slots representing bit 0's.

As seen from (6.19), $i_{sp-sp}(\tau_n)$ is a function of the ASE noise; thus, $i_{sp-sp}(\tau_n)$ also gives rise to signal fluctuation. By using the fact that x, y, $\tilde{x}$, and $\tilde{y}$ are independent, and that $\text{var}[x^2] = 2\,\text{var}^2[x]$ for a Gaussian random process, the variance of $i_{sp-sp}(\tau_n)$ can be written as

$$\text{var}\left[i_{sp-sp}(\tau_n)\right] = 2\mathcal{R}^2\sigma_x^4. \tag{6.29}$$

Since the bandwidth of $i_{sp-sp}(\tau_n)$ is approximately $B_0/2$, the variance of the spontaneous-spontaneous beat noise referred to the photodiode output can be written as

$$\sigma_{sp-sp}^2 = 2\mathcal{R}^2\sigma_x^4 \frac{B_e}{B_0/2}. \tag{6.30}$$

By substituting (6.2) and (6.15) into (6.30), σ_{sp-sp}^2 becomes

$$\sigma_{sp-sp}^2 = 4\left[\eta q_e n_{sp}(G-1)\right]^2 B_0 B_e. \tag{6.31}$$

When all contributed noises are assumed to be uncorrelated, the total variance of the noise referred to the photodiode output is the sum of the variances of individual noises. That is, σ_1 and σ_0 can be evaluated from

$$\sigma_1^2 = \sigma_{th}^2 + \sigma_{q-sp,1}^2 + \sigma_{sp-sp}^2 , \tag{6.32}$$

and

$$\sigma_0^2 = \sigma_{th}^2 + \sigma_{q-sp,0}^2 + \sigma_{sp-sp}^2 . \tag{6.33}$$

In practice, the gain of the preamplifier G is large; thus, both σ_{q-sp}^2 and σ_{sp-sp}^2 are approximately proportional to G^2 [see (6.27), (6.28) and (6.31)]. As a result, the thermal noise at the receiver is negligible. In that case, (6.32) and (6.33) can be written as

$$\sigma_1^2 = G^2 \left[2\eta^2 q_e \left(\frac{q_e}{h\nu} \right) n_{sp} B_0 P_{r,1} \frac{B_e}{(B_e + B_0/2)} + 4\left(\eta q_e n_{sp} \right)^2 B_0 B_e \right] \tag{6.34}$$

and

$$\sigma_0^2 = G^2 \left[2\eta^2 q_e \left(\frac{q_e}{h\nu} \right) n_{sp} B_0 P_{r,0} \frac{B_e}{(B_e + B_0/2)} + 4\left(\eta q_e n_{sp} \right)^2 B_0 B_e \right]. \tag{6.35}$$

Note that Q calculated semi-analytically from (6.11) is independent of the preamplifier gain G. This is because both the eye opening EOP [see (6.17)], and the standard deviations (σ_1 and σ_0) are proportional to G, hence, canceling G out. The system performance in terms of Q is then evaluated by numerically determining the eye opening at the decision time, and calculating σ_1 and σ_0 by using (6.34) and (6.35).

Although the optical preamplifier introduces an additional noise to the receiver, the preamplifier in general improves the system performance due to the preamplification of the signal and suppressing the subsequent noise at the receiver. This implies that the maximum transmission distance can be increased by employing an optical preamplifier. In order to extend the transmission distance further, in-line optical amplifiers are required to periodically compensate for the loss along the transmission line. Similar to the preamplifier, those in-line optical amplifiers also act as additional noise sources. The analysis of systems employing the in-line optical amplifiers is discussed in the next section.

6.2.2 Multiple-Span Systems with In-line Optical Amplifiers and Optical Preamplifier

When the effect of dispersion is negligible, the eye degradation is mainly due to the fiber loss. If the transmission distance is extremely large, the signal power at the receiver could be so weak that the transmitted data cannot be recovered successfully at the receiver. Increasing the transmitted power is one solution, but it is limited by the available power at the transmitter and the fiber nonlinearity. The practical solution is to employ in-line optical amplifiers to regularly compensate for the fiber loss. The schematic diagram of a system employing in-line optical amplifier is shown in Fig. 6.2b. It consists of M spans of optical fibers with optical amplifiers placed periodically along the transmission path to boost the signal power. The optical preamplifier is also employed at the end of the transmission link to further improve system performance. Similar to the case of single-link systems, the preamplifier is followed by the optical bandpass filter to limit the ASE noise. It should be noted that there is no optical bandpass filter at the output of each in-line optical amplifier since it is necessary to amplify all channels simultaneously in WDM systems. Moreover, the gain of each in-line amplifier is assumed to be independent of the input signal power. Each span has a total length of L_k km where the subscript k is used to indicate the span number. It should be noted that the lengths (or total losses) of individual spans are not restricted to be identical. The ASE noise power in one polarization at an in-line amplifier output is still governed by (6.15) with G being replaced by the gain of the considered in-line optical amplifier.

In order to calculate the accumulated ASE noise at the receiver, the gain of each in-line optical amplifier has to be determined. However, the accumulated ASE noise at the receiver can be made independent of the gains of the in-line optical amplifiers if the gain of the k^{th} in-line optical amplifier is chosen to be

$$G_k = e^{\alpha_{k+1} L_{k+1}}, \tag{6.36}$$

where α_{k+1} is the loss in the units of nepers/km for the $k+1^{th}$ span. That is, the gain of the k^{th} in-line optical amplifier in the transmission path is assumed to be equal to the reciprocal of the loss of the fiber span following that amplifier. At the input of the $k+1^{th}$ in-line optical amplifier, the ASE noise due to the k^{th} in-line optical amplifier is

attenuated by $1/G_k$. Since the amplifier gain G_k is usually large, the factor $(G_k - 1)$ in (6.15) can be approximated to be equal to G_k. Hence, For *M* spans which corresponds to $M-1$ in-line optical amplifiers, it can be shown that the power spectral density of the accumulated ASE noise at the fiber output is equal to $(M-1)n_{sp}h\nu$. When the ASE noise due to the optical preamplifier and the effect of the optical filter having the bandwidth B_0 are taken into account, the accumulated ASE noise in one polarization at the photodiode input is approximately governed by

$$P_{ASE} = Mn_{sp}h\nu(G-1)B_0, \tag{6.37}$$

where G is the gain of the optical preamplifier at the receiver. Note that with this assumption, the signal powers at the input of individual in-line optical amplifiers are identical. It is clearly seen from (6.37) that the accumulated ASE noise at the receiver is independent of the gains of the in-line amplifiers, and that the accumulated ASE noise increases linearly with the total number of spans M. The calculation of Q is similar to the case of single-span systems employing optical preamplifiers with (6.37) being used instead of (6.15). The modifications in the analytical expressions of σ_1 and σ_0 are explained as follows.

In the previous section where a single optical amplifier is employed as a preamplifier, the variances of the ASE noise components x, y, $\tilde{x}$ and $\tilde{y}$ at the preamplifier output are governed by (6.15). Those variances are each equal to the ASE noise power in one polarization. Consequently, for a system having M optical amplifiers, the variance of the signal-spontaneous beat noise can be found by replacing σ_x^2 in (6.22) with $M\sigma_x^2$ whereas the expression of σ_x^2 is still given by (6.15). By doing so, (6.27) and (6.28) becomes

$$\sigma_{q-sp,1}^2 = 2M\eta^2 q_e\left(\frac{q_e}{h\nu}\right)G(G-1)n_{sp}B_0P_{r,1}\frac{B_e}{(B_e+B_0/2)}, \tag{6.38}$$

and

$$\sigma_{q-sp,0}^2 = 2M\eta^2 q_e\left(\frac{q_e}{h\nu}\right)G(G-1)n_{sp}B_0P_{r,0}\frac{B_e}{(B_e+B_0/2)}. \tag{6.39}$$

As seen from (6.38) and (6.39), the variances of the signal-spontaneous beat noises for a system employing in-line amplifiers and a preamplifier are M times larger those for a system employing only an optical preamplifier.

Similarly, σ_{sp-sp}^2 can be found by modifying (6.30), and the final expression of σ_{sp-sp}^2 in this case is given by

$$\sigma_{sp-sp}^2 = 4\left[M\eta q_e n_{sp}(G-1)\right]^2 B_0 B_e. \tag{6.40}$$

Unlike $\sigma_{q-sp,1}^2$ and $\sigma_{q-sp,0}^2$, σ_{sp-sp}^2 for this system is a function of M^2. Thus, for large M, the spontaneous-spontaneous beat noise is the dominant noise source at the receiver. By substituting (6.38), (6.39) and (6.40) into (6.32) and (6.33) where appropriate, and neglecting the thermal noise at the receiver, the variances for bit 1 and bit 0 for a system employing in-line amplifiers and a preamplifier are given by

$$\sigma_1^2 = G^2\left[2M\eta^2 q_e\left(\frac{q_e}{h\nu}\right)n_{sp}B_0 P_{r,1}\frac{B_e}{(B_e+B_0/2)} + 4\left(M\eta q_e n_{sp}\right)^2 B_0 B_e\right] \tag{6.41}$$

and

$$\sigma_0^2 = G^2\left[2M\eta^2 q_e\left(\frac{q_e}{h\nu}\right)n_{sp}B_0 P_{r,0}\frac{B_e}{(B_e+B_0/2)} + 4\left(M\eta q_e n_{sp}\right)^2 B_0 B_e\right]. \tag{6.42}$$

It is clearly seen from (6.41) and (6.42) that the accumulation of the ASE noises caused by in-line amplifiers results in higher signal fluctuation compared with systems employing only an optical preamplifier. However, in-line optical amplifiers incorporated with an optical preamplifier allow longer transmission distance.

Up to this point, the mathematical expressions used for semi-analytically calculating Q are derived for all types of system configurations: single-span systems with/without optical preamplifiers, multiple-span systems employing in-line optical amplifiers and preamplifiers. In the following sections, the performance improvements offered by various optical modulation formats are compared. It should be noted, however, that Q is not the only criterion used for evaluating the performance improvement obtained from each modulation format compared with a conventional RZ with no PM. The eye profile at the receiver is another performance measure. Since all the optical modulation formats considered are based on RZ pulse shapes, the eye profiles at the

receiver should still be RZ. The deviation of the eye profile from RZ may cause errors in the synchronization between the received signal and the local clock. Both Q and the eye profile at the receiver are two performance measures used in the investigations discussed in the remaining sections of this chapter.

6.3 SINGLE-SPAN SYSTEMS WITHOUT OPTICAL PREAMPLIFIERS

In this section, single-span systems employing a dispersion- shifted fiber (DSF) are investigated. The system configuration simply consists of a transmitter, an optical fiber, and a receiver. The optical modulation formats considered in the investigation are sinusoidal alternating phase modulation (APM), sinusoidal same phase modulation (SaPM), square wave phase modulation (SWM), continuous-wave square-wave (CWSW), optical duobinary, alternate mark inversion (AMI), and a conventional RZ format with no PM (No PM). The purpose of this investigation is to gain understanding on how each modulation format performs in a practical system where an optical fiber is not linear and lossless.

In terms of the transmitter configuration, optical duobinary and its variant, AMI, differ from the other types of modulation format because both formats require encoders to achieve signal characteristic suitable for transmission. Shown in Fig. 6.3a is the transmitter configuration of APM, SaPM, SWM, and CWSW signal formats, and corresponding phase characteristics. It should be noted that in the case of the CWSW signal format, the CW signal from the laser is fed directly to the phase modulator (the RZ modulator is removed from the block diagram shown in Fig. 6.3a), which is driven by square-wave phase function similar to the SWM signal format. The block diagram of the transmitter for the optical duobinary and AMI signal formats is shown in Fig. 6.3b. For the optical duobinary signal format, the encoder is a delay-and-add circuit whereas the delay-and-subtract circuit is used as the encoder in the case of the AMI signal format. In the case of no PM (conventional RZ) format, the NRZ data (in Fig. 6.3b) is fed directly to the data modulator consistent with [56]. For the optical duobinary, AMI and no PM signal formats, an optical bandpass filter having a bandwidth BW_{Tx} is placed at the fiber

input to limit the signal bandwidth as shown in Fig. 6.3b. Note that the transmitter filters are taken to be fifth order Butterworth filters for all modulation formats and that the filter bandwidth is normalized by the bit rate for ease of visualization. In WDM systems high order filters are preferable in order to reduce the cross talk among channels.

The DSF used in the system simulations has a nonlinear refractive index of 3×10^{-20} m^2/W, an effective core area of 70 μm^2, and a loss of 0.2 dB/km. The value of dispersion coefficient D considered here is -0.5 ps/(km·nm). The normalized transmitter filter bandwidth BW_{Tx} in this simulation is set to 2, and the average transmitted power is set to 6 dBm (4 mW) for all modulation formats considered. A 3rd order Butterworth filter having a bandwidth of 30 GHz is used to model the electrical lowpass filter at the receiver. In this case, the only noise source in the system is the thermal noise at the receiver. Shown in Fig. 6.4 are the eye diagrams and corresponding Q at the receiver output when $z = 100$ km and $D = -0.5$ ps/(km·nm). The corresponding worst-case bit patterns when nearest neighboring bits are considered are also summarized in Table 6.1. It is seen from Fig. 6.4g that in the case of no PM, the growth of spurious pulses midway between adjacent pulses representing bit 1's is significant. With no PM there is severe distortion caused by the dispersion and nonlinearity, making the eye no longer RZ. In addition, the tail of an adjacent pulse may destructively interfere with the center of another pulse due to both components being out of phase, hence severely reducing the signal level at the center of the pulse ($\tau_n = 0$). This in effect decreases the signal level for bit 1;thus, the Q value is degraded to be well below the threshold value of 15.6 dB.

6.3.1 APM and SaPM

In the case of APM signal format (Fig. 6.4a), adjacent pulses having opposite chirps can prevent the growth of spurious pulses; therefore, the eye profile is still RZ. Because adjacent pulses have opposite chirps, some pulses are broadened more severely than others. Unlike no PM, the tail of an adjacent pulse does not destructively interfere with the center of another pulse due to the fact that both pulses have opposite phase variation. Therefore, the worst-case bit pattern for bit 1 in this case is 010, which

corresponds to an isolated pulse having the wrong chirp. The destructive interference between adjacent pulses (bit pattern 111) in the case of no PM is more severe than the effect of wrong chirp. Consequently, the APM signal format also performs better than no PM in terms of the Q value by 2.8 dB.

Similar to no PM, the spurious pulses are not eliminated in the case of SaPM as shown in Fig. 6.4b because adjacent pulses have identical phase variation. In addition, the tail of an adjacent pulse destructively interferes with the center of another pulse; therefore, the worst-case bit pattern for bit 1 in this case is 111. This implies that at large transmission distance, the pulse compression effect is not effective in delaying the growth of spurious pulses. The eye profile of SaPM is similar to that of no PM; however, delaying the growth of spurious pulses still improves the Q value.

6.3.2 SWM and CWSW

As seen from Fig. 6.4c, which corresponds to the SWM signal format, 180° phase inversion between adjacent bit slots effectively suppresses the growth of spurious pulses. The eye profile in this case is still RZ, and the Q value is 4.4 dB better than that of no PM. When the eye diagrams shown in Fig. 6.4c and Fig. 6.4d are compared, the eye profiles for the SWM and CWSW signal formats are nearly identical. This is due to the fact that for both signal formats adjacent pulses have opposite signs. However, the tail of an adjacent pulse interferes constructively with the center of another pulse; therefore, the worst-case bit pattern for bit 1 is not 111 but 010 for both SWM and CWSW signal formats. A long string of bit 1's (bit pattern $\cdots 111 \cdots$) corresponds to the top rail in the eye diagram.

When an isolated pulse (bit pattern $\cdots 010 \cdots$) is considered, its peak (lowest signal level for bit 1 at $\tau_n = 0$) in the case of CWSW is higher than that of SWM because of the peak intensity enhancement (PIE). Therefore, in terms of Q the CWSW format outperforms SWM. In addition, both CWSW and SWM signal formats have nearly the same signal variations on empty bit slots (the bottom rails in the eye diagrams). This implies that the broad pedestals of a CWSW pulse do not deteriorate the eye opening.

The PIE results in 0.7 dB better performance in terms of Q when CWSW is compared with SWM.

6.3.3 Optical Duobinary and AMI

Recall from Chapter 3 that for the optical duobinary signal format adjacent pulses always have identical sign. Therefore, the growth of spurious pulses is not suppressed, which can be seen in Fig. 6.4e. The eye profile of the optical duobinary signal format is similar to that of the no PM format. That is, the dispersion and nonlinearity severely distort the signal so that the eye is no longer RZ. Since adjacent pulses have identical sign similar to the case of no PM, the worst-case bit pattern for bit 1 is 111. In addition, the performance of the optical duobinary signal format in term of Q is poorer than the no PM. This is due to the fact that the spectral width of the optical duobinary is not narrower than that of the no PM signal format as discussed in Chapter 3. In order for the optical duobinary signal format to provide performance improvement, the transmitter filter bandwidth BW_{Tx} has to be sufficiently small to reduce the effect of dispersion. For the optical duobinary signal format, the transmitted blocks of pulses surrounding an empty bit slot have opposite signs; therefore, it is more robust to ISI caused by the transmitter filter than the no PM format.

Although the hardware configurations at the transmitter for the optical duobinary and AMI signals are similar except for the arithmetic operation in the encoding process, AMI provides significant performance improvement compared with optical duobinary. Unlike the optical duobinary signal, the eye profile of the AMI signal remains RZ as shown in Fig. 6.4f. This is because consecutive transmitted pulses have opposite signs regardless of the number of empty bit slots in between for the AMI signal. The eye profile and the worst-case bit pattern for bit 1 of the AMI signal are similar to those of the SWM and CWSW signals. In terms of Q, AMI outperforms the optical duobinary by 5 dB. It should be noted that the worst-case bit pattern for bit 0 is always 101 independent of the optical modulation format as shown in Table 6.1. This can be intuitively understood from the fact that a bit 0 is represented by an empty bit slot; thus, the ISI is

most severe when that empty bit slot is surrounded by pulses. The dispersion causes those pulses to spread into that empty bit slot, hence creating the ISI.

6.3.4 Performance Comparisons

The system performances in terms of Q for all modulation formats at different transmitter filter bandwidth BW_{Tx} are summarized in Table 6.2. Note that the optimum modulation indices for APM and SaPM are listed in parentheses. In the case of no PM, the system performance degrades with the increase in BW_{Tx}. This is due to the fact that the effect of dispersion increases with the signal bandwidth. Narrowband filtering at the transmitter converts the no PM signal from RZ to NRZ, which improves Q because NRZ is generally more robust to dispersion than RZ. It should be noted, however, that NRZ is more susceptible to interchannel impairments than RZ as discussed in Chapter 3.

Similar to no PM, Q decreases with the increase in BW_{Tx} for APM, SaPM, SWM, and optical duobinary. In the case of AMI, it is found that the optimum BW_{Tx} is 1.5. In contrast to the other modulation formats considered, the system performance in the case of CWSW signal format increases with BW_{Tx}. This is due to the fact that dispersion is required to achieve PIE, and that the effect of dispersion increases with the signal bandwidth. Although the SaPM signal format can achieve the highest Q at $BW_{Tx} = 1$ as shown in Table 6.2, the eye profile at the receiver is no longer RZ. When the shape of the eye profile is considered as a criterion (see Fig. 6.4), APM, SaPM, and optical duobinary signal formats are significantly inferior to CWSW. The eye profile of the CWSW signal format always remains RZ independent of the transmitter filter bandwidth. In spite of the fact that the eye profile of SWM resembles that of CWSW, a CWSW pulse can undergo PIE during propagation given that BW_{Tx} is not too small. This causes CWSW to outperform SWM at large BW_{Tx} as shown in Table 6.2. It should be noted, however, that CWSW and SWM are comparable at small BW_{Tx}. This is due to the fact that at such small BW_{Tx}, a CWSW pulse resembles a SWM pulse.

Compared with the AMI signal format, the optical duobinary performs better at small BW_{Tx}. Similar to no PM, narrowband filtering at the transmitter causes the optical duobinary signal to be NRZ. For AMI, the alternate sign between successive pulses prevents the conversion from RZ to NRZ, and narrow band filtering leads instead to timing jitter on the transmitted pulses. Hence, the Q value of the AMI signal is degraded and is poorer than that of optical duobinary when $BW_{Tx} = 1$. However, the eye profile of the AMI signal is superior to that of optical duobinary, which is NRZ.

When an optical preamplifier is employed, the noise-limited maximum transmission distance is longer, which means that the eye degradations from dispersion and nonlinearity are more severe. For the transmitter configuration shown in Fig. 6.3a, CWSW performs significantly better than APM and SaPM in terms of the eye profile. The eye profile of CWSW remains RZ regardless of the transmitter filter bandwidth while Q is improved. When SWM and CWSW are compared, CWSW can achieve PIE, which further improves the system performance in term of Q. Therefore, APM, SaPM and SWM are not investigated further. For the transmitter configuration shown in Fig. 6.3b, the AMI signal format noticeably outperforms the optical duobinary in terms of Q and the eye profile provided that the transmitter filter bandwidth is not too small. Therefore, the following investigations will be focused on the performance comparisons between CWSW and AMI, with no PM still considered for reference purposes.

6.4 SINGLE-SPAN SYSTEM EMPLOYING OPTICAL PREAMPLIFIER [146]

The eye profiles of CWSW and AMI still being RZ in shape implies that the maximum transmission distance can be extended farther by employing an optical preamplifier. The schematic diagram of this system is shown in Fig. 6.2a. Simulations of a single-channel system employing an optical amplifier are performed to determine the system parameters that maximize the transmission distance z. The range of the normalized filter bandwidth at the transmitter BW_{Tx} that we consider is from 1 to 4. The average transmitted power is varied from 3 dBm to 12 dBm. The values of the dispersion

considered are ± 0.5 ps/(km·nm). The optical amplifier is assumed to have a noise figure F_n of 6 dB (corresponding to $n_{sp} = 2$), and the normalized bandwidth of the optical bandpass filter at the preamplifier output is set to 2 (80 GHz). Similar to the optical filter at the transmitter, a fifth order Butterworth is used to model the optical filter at the preamplifier output. The gain of the optical preamplifier G is assumed to be sufficiently high that subsequent receiver thermal noise is negligible compared with the amplified spontaneous emission (ASE) noise from the preamplifier. The other system parameters remain unchanged. We investigate the range of BW_{Tx} from 1 to 4 because if BW_{Tx} is made narrower than 1, a higher power laser would be required to compensate for the loss caused by the filter in order to maintain the same P_{avg} at the fiber input. Moreover, the filter severely distorts the RZ signal so that it is no longer RZ at small filter bandwidth. A filter bandwidth greater than 4 is essentially no filtering at all. Large signal bandwidth is not desirable in WDM systems.

Shown in Fig. 6.5 is the plot of the value of Q as a function of the average transmitted power P_{avg} when $D = +0.5$ ps/(km·nm), $BW_{Tx} = 4$, and $z = 190$ km. At low transmitted power P_{avg}, the systems experience low signal to noise ratio. Since the effect of fiber nonlinearity increases with the signal power P_{avg}, the waveform distortion caused by the interaction between the dispersion and nonlinearity is severe at high transmitted power. Hence, there exists an optimum transmitted power $P_{avg,Opt}$ for given D, z, and BW_{Tx} as shown in Fig. 6.5. At the optimum transmitter power the Q value for CWSW is found to be equal to 16.9 dB, which is above the threshold value of 15.6 dB. On the other hand, the Q values of both AMI and no PM are well below the threshold, which implies that the probability of bit error for systems employing AMI and no PM signal formats is higher than 10^{-9} at this transmission distance. Another conclusion that can be drawn from Fig. 6.5 is that CWSW is more robust to the nonlinearity than AMI and no PM due to higher allowed value of $P_{avg,Opt}$. This is because for a given P_{avg}, the pulse peak power for CWSW at the fiber input is lower than those of AMI and no PM due to the fact that CWSW pulse is flatter and has steeper edges than those of AMI and no PM; thus, CWSW

allows higher P_{avg}. Having this property as well as PIE, CWSW outperforms AMI and no PM over the whole range of considered P_{avg}.

As stated earlier, an additional system parameter that we consider in maximizing the system performance is the optical filter bandwidth at the transmitter BW_{Tx}. The value of Q as a function of BW_{Tx} is plotted in Fig. 6.6 for $D = +0.5$ ps/(km·nm), $P_{avg} = 8$ dBm, and $z = 190$ km. As one may expect, narrower BW_{Tx} yields better system performance in the case of no PM due to severe dispersion at large transmission distance z. The higher signal distortion caused by the narrow filter bandwidth BW_{Tx} is traded for the less detrimental effect of dispersion. For AMI, the optimum transmitter filter bandwidth BW_{Tx} is found to be equal to 1.5. The existence of the optimum filter bandwidth is due to the balance between the effect of dispersion and the waveform distortion caused by the transmitter filter. The alternate-sign between successive pulses possessed by AMI results in the AMI being more robust to the effect of dispersion than no PM, thus allowing larger transmitter filter bandwidth.

In contrast to AMI and no PM, increasing BW_{Tx} improves the value of Q for CWSW. This can be explained as follows. The PIE requires a sufficient degree of dispersion, which increases with the signal bandwidth. Therefore, larger BW_{Tx} is preferable, when the transmission distance is still within the range in which the PIE is still effective. Moreover, increasing BW_{Tx} lowers the pulse peak power, which in effect reduces the effect of nonlinearity. The increase in Q with BW_{Tx} in the case of CWSW also implies that CWSW is more resistant to the effect of dispersion than AMI and no PM. When AMI and no PM are compared, the Q value of no PM degrades with the increase in BW_{Tx} more rapidly than that of AMI. This indicates that AMI is more robust to dispersion than no PM.

In order to understand how dispersion and nonlinearity at different transmission distance affect the system performance and system parameters, additional simulations were conducted. The optimum transmitted power $P_{avg,Opt}$ and the normalized filter bandwidth BW_{Tx} that maximize the Q value at various transmission distance z are listed

in Table 6.3 and 6.4 when $D = +0.5$ ps/(km·nm) and $D = -0.5$ ps/(km·nm), respectively. It is clearly seen from Table 6.3 and 6.4 that the BW_{Tx} that maximizes Q decreases with increasing z for AMI and no PM in order to minimize the effect of dispersion. In the anomalous dispersion regime [$D = +0.5$ ps/(km·nm)], the CWSW signal format can achieve a maximum transmission distance of 195 km, which is the best of all the signal formats. In the case of AMI and no PM, the corresponding maximum transmission distances are 187 km and 179 km, respectively.

At the optimum parameters shown in the bottom of Table 6.3 for AMI when $z = 187$ km ($BW_{Tx} = 1.5$, $P_{avg,Opt} = 8$ dBm), AMI performs better than CWSW by only 0.6 dB. The corresponding Q value for AMI is 15.6 dB compared with 15.0 dB and 10.7 dB for CWSW and no PM, respectively. However, the system performance for CWSW increases with BW_{Tx}; therefore, CWSW becomes comparable to AMI when BW_{Tx} is larger than 1.5, and better than AMI at large BW_{Tx}. At $BW_{Tx} = 2.5$, the Q value of CWSW becomes 15.5 dB, which is comparable to that of AMI (15.6 dB at $BW_{Tx} = 1.5$) with the same transmitted power. When $BW_{Tx} = 4$ and $P_{avg} = 8$ dBm (optimum transmitted power for AMI), the Q value for CWSW is 16.4 dB compared with 11.4 dB for AMI. It is seen that even at the optimum transmitted power for AMI ($P_{avg,Opt} = 8$ dBm in this case), CWSW performs better than AMI provided that BW_{Tx} is sufficiently large. AMI can achieve the Q value of 15.6 dB at $BW_{Tx} = 1.5$ while the Q value of CWSW is 16.4 dB at $BW_{Tx} = 4$ when the transmitted power is 8 dBm. It should be noted, however, that when $z = 187$ km, the optimum transmitted power $P_{avg,Opt}$ is 10 dBm for CWSW and the corresponding Q value is 17.7 dB.

The eye diagrams of all signal formats at $z = 195$ km (the maximum transmission distance $z_{\max}$ for CWSW when $D = +0.5$ ps/(km·nm)) are shown in Fig. 6.7. Note that $P_{avg,Opt}$ and BW_{Tx} that maximize Q for all modulation formats considered are different. It is clearly seen from Fig. 6.7a that the eye profile of CWSW is still reasonably good. In the case of AMI as shown in Fig. 6.7b, although there are no spurious pulses, the jitter

caused by the narrow transmitter filter bandwidth is apparent. The jitter in conjunction with the detrimental effects in the optical fiber limits the transmission distance in the case of AMI. Similar to AMI, no PM experiences jitter caused by the narrow filter bandwidth. However, the jitter is not noticeable because the level of the spurious pulses is significant as shown in Fig. 6.7c. The eye profile in the case of no PM is not recognizable as RZ due to severe effects of fiber dispersion. In terms of both Q and eye profile, CWSW noticeably outperforms AMI and no PM, thus allowing longer transmission distance.

When $D = -0.5$ ps/(km·nm) is considered, the maximum transmission distances for all signal formats are less than when $D = +0.5$ ps/(km·nm). This is simply because in the normal dispersion regime (D negative) the nonlinear effect in the optical fiber enhances the effect of dispersion, which results in severe waveform distortion. The adverse interaction between the dispersion and nonlinearity is increased with the transmission distance although the fiber loss reduces the effect of nonlinearity. As a consequence, $P_{avg,Opt}$ decreases with the increase in z for all signal formats as shown in Table 6.4. When $P_{avg,Opt}$ in Table 6.3 and Table 6.4 are compared, $P_{avg,Opt}$ when $D = -0.5$ ps/(km·nm) (Table 6.4) is lower than $P_{avg,Opt}$ when $D = +0.5$ ps/(km·nm) (Table 6.3) at large z due to the detrimental effect of nonlinearity. Similar to the case when $D = +0.5$ ps/(km·nm), $P_{avg,Opt}$ for CWSW is higher than those of the other signal formats when $D = -0.5$ ps/(km·nm) at large z (160 km for example). This implies that CWSW is more tolerant to the effect of nonlinearity than AMI and no PM. In addition, the transmitter filter bandwidth BW_{Tx} that maximizes Q is still equal to 4 in the case of CWSW, indicating that PIE can help improve system performance even under the adverse effect of nonlinearity. In terms of Q, CWSW is better than AMI and no PM for all considered transmission distances at which Q is larger than 15.6 dB.

As listed at the bottom of Table 6.4, the maximum transmission distances for all modulation formats considered are comparable, which is due to the fact that the dispersion and nonlinearity severely distort the signal. The waveform distortion grows rapidly with the transmission distance z. The maximum transmission distance that CWSW signal format can achieve when $D = -0.5$ ps/(km·nm) is 162 km. The

corresponding eye diagrams for all signal formats at that distance are plotted in Fig. 6.8. It is apparent in Fig. 6.8 that among the three the eye profile of CWSW is the best. Note that the waveform distortion caused by the combined effect of dispersion and nonlinearity is noticeable. In the case of AMI, the jitter is more severe than that in the anomalous dispersion regime when Fig. 6.8b is compared with Fig. 6.7b, although the transmission distance in Fig. 6.8 is shorter. Without PM, the dispersion and nonlinearity distort the signal severely as shown in Fig. 6.8c. In terms of Q, CWSW is better than AMI by 1 dB. When the Q values of CWSW and no PM are compared, CWSW outperforms no PM by 0.5 dB. However, the eye profile of CWSW is significantly better than that of no PM, which is no longer RZ.

It is clearly seen from this investigation that CWSW provides significant performance improvement relative to AMI and no PM in systems employing DSF. The PIE and alternate sign between adjacent pulses are the key factors that cause CWSW to be resistant to the deleterious effects of fiber dispersion and nonlinearity. For a 40 Gb/s single-span system employing an optical preamplifier, the maximum transmission distances that can be achieved by employing the CWSW signal format are 195 when $D = +0.5$ ps/(km·nm) and 162 km when $D = -0.5$ ps/(km·nm). On the other hand, for AMI the maximum transmission distances are 187 km and 159 km, respectively. The eye profile of CWSW still maintains the RZ shape even at large transmission distance z.

As discussed in Chapter 2, the advantage of the DSF is due to its small dispersion; therefore, the accumulated dispersion ($D \cdot z$) is not so large that dispersion compensation is necessary to reduce the effect of dispersion. However, in WDM systems employing DSF, channel spacing has to be large to avoid interchannel impairments, such as cross-phase modulation (XPM) and four-wave mixing (FWM), making the bandwidth utilization inefficient. In order to pack WDM channels more effectively, an optical fiber having larger dispersion than the DSF is required. In the following sections, single-channel systems employing transmission fibers whose dispersions are larger than that of the DSF are investigated in order to thoroughly understand how dispersion and nonlinearity affects system performance in such systems.

6.5 SINGLE-SPAN DISPERSION-MANAGED SYSTEM EMPLOYING OPTICAL PREAMPLIFIER

Employing an optical fiber having large dispersion as a transmission fiber is advantageous in terms of minimizing interchannel impairments. However, large local dispersion implies large accumulated dispersion, which causes the effect of dispersion to be intolerable. Thus, dispersion management is required in such systems to offset the accumulated dispersion, especially in high bit rate systems. Due to the fact that the dispersion and nonlinearity impact the signal simultaneously, there are still intrachannel impairments in dispersion-managed systems as discussed in Chapter 3. Those impairments are intrachannel four-wave mixing (IFWM) and intrachannel cross-phase modulation (IXPM). Recall that the IFWM among overlapping pulses during propagation results in the growth of ghost pulses and amplitude jitter (see Fig. 3.3). On the other hand, IXPM among overlapping pulses causes the shift in the mean frequency of the interacting pulses, leading to the timing jitter. Undoubtedly, both IFWM and IXPM degrade the system performance in terms of Q and the eye profile at the receiver in dispersion-managed systems.

In this section, a system employing dispersion management to reduce the effect of dispersion is studied. For simplicity, a single-span, single-channel system employing an optical preamplifier is considered similar to the previous section. The system parameters remain unchanged except for the optical fiber. In terms of dispersion, two types of transmission fibers are investigated: ones with moderate and large local dispersions. Shown in Fig. 6.9 are the fiber configurations numerically investigated in this section. The curve (a) corresponds to the system in which the transmission fiber has moderate local dispersion. In this case, a TrueWave™ reduced slope fiber (TRSF) having the dispersion D of +4 ps/(km·nm) is used to represent the transmission fiber having moderate local dispersion. At the preamplifier input perfect dispersion compensation is performed by inserting a dispersion compensating fiber. Due to its large negative dispersion, an extra-high-slope dispersion compensating (EHS-DK) fiber having a dispersion of –232 ps/(km·nm) is used as the dispersion compensating fiber. The length

of the EHS-DK fiber is adjusted so that the accumulated dispersion at the preamplifier input is returned to zero.

The curve (b) in Fig. 6.9 corresponds to the transmission fiber having large local dispersion. A standard single-mode fiber (SSMF) having the dispersion of +17 ps/(km·nm) is used as the transmission fiber in this case. Similar to the system employing TRSF, the EHS-DK fiber is deployed at the preamplifier input to reset the accumulated dispersion back to zero. Due to the fact that the dispersion of SSMF is approximately four times larger than that of TRSF, a longer length of the EHS-DK fiber is required in the case of SSMF. Since the dispersion compensating fiber is not lossless, a longer length of fiber implies higher additional loss. One approach to avoid such high additional loss associated with long length of dispersion compensating fiber is to perform dispersion compensation within the transmission span. This approach corresponds to the curve (c) in Fig. 6.9. In this fiber configuration, two types of fibers are employed as transmission fibers. The first transmission fiber is still SSMF. The second transmission fiber not only acts as a transmission fiber, but also performs dispersion compensation. In general, the second transmission fiber is a reverse-dispersion fiber (RDF) whose dispersion is –26.91 ps/(km·nm). The lengths of SSMF and RDF are tailored so that the accumulated dispersion is zero at the preamplifier input. It should be noted that in all three types of fiber configurations considered, the accumulated dispersion at the preamplifier input is set to zero in order to understand how optical modulation formats improve system performance without the effect of residual dispersion, which is not investigated in this dissertation. The main objective is to study the drawbacks and advantages of each transmission configuration in terms of optimum system parameters and intrachannel impairment suppression.

6.5.1 Moderate Local Dispersion with Modular Dispersion Compensating Fiber

In this case, the transmission fiber is TRSF. The TRSF used in the system simulations has a dispersion of +4 ps/(km·nm), a nonlinear refractive index of 2.7×10^{-20} m^2/W, an effective core area of 55 μm^2, and a loss of 0.2 dB/km. The EHS-DK fiber used as a modular dispersion compensating fiber at the receiver has a dispersion of –232

ps/(km·nm), a nonlinear refractive index of 2.7×10^{-20} m^2/W, an effective core area of 19 μm^2, and a loss of 0.59 dB/km. Listed in Table 6.5 are the optimum system parameters that maximize the Q value at various transmission distances z (length of TRSF fiber).

6.5.1.1 Optimum Transmitted Power

It is clearly seen from Table 6.5 that for all modulation formats considered, the optimum transmitted power $P_{avg,Opt}$ initially decreases with the increase in transmission distance z. However, at large z the optimum transmitted power $P_{avg,Opt}$ increases with z. This can be explained as follows. At short z, the loss and pulse spread caused by the main transmission fiber (TRSF) are so small that the signal entering the EHS-DK fiber still has high intensity. Since the level of nonlinearity of the EHS-DK fiber is high (due to its small effective core area), the nonlinear impairments are strong. Although increasing z means higher loss and larger accumulated dispersion, which reduces the signal intensity, the length of the EHS-DK fiber is longer to return the accumulated dispersion back to zero. Longer length of EHS-DK fiber provides a longer interaction length for the nonlinearity to affect the signal. Therefore, at short z, $P_{avg,Opt}$ decreases with the increase in z to reduce the nonlinear effects in the EHS-DK fiber. However, when the transmission distance z is large, the loss in the main transmission fiber is high and a pulse spreads severely during the propagation in the transmission fiber (TRSF) due to large accumulated dispersion. Thus, the signal intensity at the input to the EHS-DK fiber is sufficiently small that the adverse effect of nonlinearity is no longer severe. That is, when the transmission distance z is sufficiently large, the EHS-DK fiber becomes more linear due to high loss and large accumulated dispersion in the main transmission fiber.

Since the accumulated dispersion is compensated and the effect of nonlinearity in the EHS-DK is small, the fiber loss becomes the limiting factor at large z. Therefore, the optimum transmitted power $P_{avg,Opt}$ increases with z to compensate for the fiber loss when z is sufficiently large for all modulation formats considered. This trend is similar to a loss-limited system where fiber loss can be compensated by increasing the transmitted power. It is found that the maximum transmission distances $z_{\max}$ for CWSW

and AMI are 206 km and 208 km, respectively, while it is equal to 200 km for no PM. However, the maximum transmission distance is still less than that of the loss-limited transmission distance, which is found to be equal to 228 km for both CWSW and AMI signal formats, and 219 km for no PM at the optimum system parameters listed at the bottom of Table 6.5. The differences in the maximum transmission distances that can be achieved in this case from the loss-limited transmission distances are primarily due to the nonlinearity, which cannot be compensated, and due to the additional loss associated with dispersion compensation process.

6.5.1.2 Optimum Transmitter Filter Bandwidth

The strong effect of nonlinearity at small z is also evident from the fact that the transmitter filter bandwidth BW_{Tx} that maximizes Q when $z = 20$ km is smaller than those at larger z as shown in Table 6.5 for AMI and no PM. Note that the optimum transmitter filter bandwidth for CWSW will be discussed later. Plotted in Fig. 6.10 are the eye diagrams for AMI signal format at different transmitter filter bandwidths BW_{Tx} when $z = 20$ km and $P_{avg,Opt} = 15$ dBm. Recall from Chapter 3 that IXPM is strongest when pulses partially overlap [see (3.2) or Fig. 3.4]. On the other hand, IFWM increases with the pulse overlaps. Since the transmission distance z (length of TRSF) is short and the local dispersion is moderate, pulses spend significant amount of time partially overlapped compared with the total transmission time. Partial overlaps between pulses in conjunction with high signal power results in severe effect of IXPM (timing jitter) as well as IFWM (amplitude jitter) as shown in Fig. 6.10a. It is clearly seen that the effect of IXPM is significant at large BW_{Tx}. Generally, there are two approaches to reduce the effect of IXPM: decreasing the overlaps or making pulses severely overlap. In general, IXPM depends on two factors: the level of pulse overlap and the intensity derivative of the interacting pulses. In fact, the effect of IXPM is strongest when interacting pulses partially overlap due to the balance between the level of overlap and the intensity derivative of the interacting pulses. The reduction of IXPM at strong pulse overlap is due to the fact that the intensity derivative of the pulses is small when the pulse overlap is strong as discussed in Chapter 3. However, the accumulated dispersion in this case is not

sufficient to induce severe pulse broadening at short transmission distance. Therefore, to decrease the effect of IXPM, pulse overlaps have to be reduced. Since the effect of dispersion is proportional to signal bandwidth, the overlaps can be reduced by limiting the signal bandwidth. However, if the transmitter filter bandwidth BW_{Tx} is too small, the waveform distortion caused by the filter is very severe. Thus, there exists an optimum BW_{Tx} that maximizes Q, and it is equal to 2 in this case. The eye diagram at $BW_{Tx} = 2$ is plotted in Fig. 6.10b. When Figs. 6.10a and 6.10b are compared, it is seen that the effect of IXPM is significantly reduced when $BW_{Tx} = 2$. The optimum BW_{Tx} is due to the trade off between waveform distortion caused by the filter at the transmitter, and the effect of IXPM. Note that this explanation is also applicable for no PM.

However, at large z where the accumulated dispersion is large, large BW_{Tx} is preferable. This can be explained as follows. In this case, the transmission fiber is TRSF whose local dispersion is moderate. Thus, pulses do not spread quickly as the transmission distance increases compared with the transmission fiber having large local dispersion, such as SSMF. Thus, pulses spend longer time partially overlapping each other in this case than when SSMF is employed as the transmission fiber. As a consequence, the dominant intrachannel impairment is IXPM. In order to reduce the time during which pulses partially overlap, pulses have to be dispersed as fast as possible. At large transmission distance z, the accumulated dispersion is sufficient to cause severe pulse spread. Hence, the transmitter filter having wide bandwidth is beneficial at large z in the case of AMI and no PM.

In the case of CWSW, BW_{Tx} that maximizes Q is always equal to unity regardless of the transmission distance z as listed in Table 6.5. This is due to the fact that the pulse peak decreases with the increase in BW_{Tx}. The pulse peak in fact represents the signal level for bit 1. Plotted in Fig. 6.11 are the eye diagrams of CWSW signal at $BW_{Tx} = 4$ and $BW_{Tx} = 1$ when $z = 200$ km and $P_{avg,Opt} = 10$ dBm. Although the effect of IXPM (timing jitter) is less at $BW_{Tx} = 4$, the eye opening when $BW_{Tx} = 4$ is significantly narrower than that corresponding to when $BW_{Tx} = 1$ at the same transmitted power. This indicates that reduction in pulse peak representing the signal level for bit 1 at large BW_{Tx}

has stronger influence on the system performance in term of Q than the decrease in IXPM at large signal bandwidth. Therefore, the transmitter filter bandwidth BW_{Tx} that maximizes Q is always equal to unity in the case of CWSW. Unlike the case of low dispersion fiber where dispersion compensation is not required and PIE results, in the case of moderate dispersion fiber with dispersion compensation there is no PIE, and consequently large BW_{Tx} is not beneficial for CWSW.

6.5.1.3 Performance Comparison

In terms of maximum transmission distance $z_{\max}$, the performances of all considered modulation formats are comparable as listed at the bottom of Table 6.5. The difference in the maximum transmission distances is not significant. Still, CWSW and AMI have longer $z_{\max}$ than no PM. It should be noted that for a given transmission distance z (200 km for example), both CWSW and AMI noticeably perform better than no PM in terms of Q. When CWSW and AMI are compared, the Q value of AMI is better than that of CWSW by only 0.4 dB at 200 km. However, CWSW has a considerably smaller transmitter filter bandwidth. Plotted in Fig. 6.12 are the eye diagrams at corresponding optimum BW_{Tx} for CWSW, AMI and no PM when $z = 206$ km ($z_{\max}$ for CWSW) and $P_{avg} = 9$ dBm (optimum transmitted power for no PM). Note that the optimum BW_{Tx} and Q are listed in the parentheses in the figure caption. It is clearly seen that the eye degradation for all modulation formats is primarily due to IXPM, causing timing jitter. Still, the effect of IFWM (amplitude jitter) is observable. In the case of no PM (Fig. 6.12c), the signal suffers the most severe IXPM. The eye profiles for both CWSW and AMI signal formats are still in very good shape. Although IXPM is independent of the signs of interacting pulses, IFWM is not. Alternate signs between adjacent pulses possessed by both CWSW and AMI reduce the effect of IFWM. The reduction in IFWM also helps decrease the effect of IXPM since both IFWM and IXPM occur simultaneously. IFWM causes intensity fluctuation among pulses. Since the effect of IXPM depends on the intensity derivative of the interacting pulses as discussed in Chapter 3, the intensity fluctuation among pulses results in asymmetric interaction among

pulses involved in the IXPM process, which in effect causes nonuniform timing shifts among pulses. Thus, the effect of IXPM is more severe when IFWM is present. This can be seen when Fig. 6.12c is compared with Figs. 6.12a and 6.12b. The eye profiles for CWSW and AMI are more symmetric and smoother than the eye profile for no PM. The phase characteristics possessed by CWSW and AMI indirectly help reduce the effect of IXPM by mean of decreasing IFWM.

Better eye profiles allow higher optimum transmitted powers $P_{avg,Opt}$ for CWSW and AMI signal formats. The eye diagrams for CWSW and AMI at corresponding optimum system parameters are plotted in Fig. 6.13. When Figs 6.13a and 6.13b are compared with Fig. 6.12a and 6.12b, it is seen that increasing the transmitted power results in higher effects of IXPM and IFWM. Nevertheless, the eye profiles for both CWSW and AMI are better than no PM even at higher transmitted power, and the dominant nonlinear impairment is still IXPM. In terms of Q, CWSW and AMI formats perform better than no PM by 1.5 dB and 1.9 dB, respectively. When the eye diagrams for CWSW and AMI are compared, the eye profiles for both signal formats are nearly identical. This suggests that the advantage of AMI over CWSW in terms of ISI for the transmission of bit 0 does not yield significant improvement. This can be understood from the fact that the dispersion of the transmission fiber is not so large that the overlaps between pulses are severe [+4 ps/(km·nm) in this case compared with +17 ps/(km·nm) for SSMF]. Both the Q values and the eye profiles indicate that the performance improvement offered by CWSW and AMI signal formats are comparable. However, the optimum transmitter filter bandwidth for CWSW is much smaller than that for AMI. The waveform distortion caused by the filter in conjunction with the effect of IXPM degrades the system performance for AMI when the filter bandwidth is small. For example, at $BW_{Tx} = 2$ the Q value for AMI reduces to 15.6 dB from 16.1 dB at $BW_{Tx} = 4$. The results suggest that the effect of IXPM can be reduced if pulses spread quickly during the propagation. It should be noted, however, that for CWSW the pulse peak at the fiber input decreases with the increase in the filter bandwidth BW_{Tx} as discussed earlier. For CWSW it is still true that the effect of IXPM can be reduced by increasing the transmitter filter bandwidth BW_{Tx}. However, the benefit of reduced IXPM at large BW_{Tx} is negated

by the reduction of the pulse peak for bit 1. This implies that the transmission fiber having large local dispersion, such as SSMF, may be beneficial in terms of minimizing IXPM. However, large local dispersion causes pulses to overlap severely, which increases IFWM. The system employing SSMF as a transmission fiber is discussed in the next section.

6.5.2 Large Local Dispersion with Modular Dispersion Compensating Fiber

In this case the transmission fiber is a standard single-mode fiber (SSMF) instead of TRSF, but the dispersion compensating fiber is still EHS-DK fiber. The SSMF has a dispersion of +17 ps/(km·nm), a nonlinear refractive index of 2.3×10^{-20} m^2/W, an effective core area of 85 μm^2, and a loss of 0.2 dB/km. Compared with TRSF, SSMF is more linear due its larger effective core area and smaller nonlinear refractive index. It should be noted that SSMF has a dispersion approximately four times larger than that of TRSF in the 1550 nm wavelength window; therefore, the effect of dispersion in SSMF is stronger. In addition, larger value of dispersion implies that a longer length of EHS-DK fiber is required for dispersion compensation in this case.

6.5.2.1 Optimum Transmitted Power

Listed in Table 6.6 are the optimum system parameters that maximize the Q value at various transmission distances z (length of SSMF fiber) when the dispersion compensating fiber is EHS-DK fiber. Similar to the previous case (TRSF and EHS-DK fiber), the optimum transmitted power $P_{avg,Opt}$ initially decreases with the increase in z. Then, $P_{avg,Opt}$ increases with z at sufficiently large z where the loss and dispersion in the transmission fiber is adequate to reduce the signal intensity down to the level at which the nonlinearity in the EHS-DK fiber does not cause severe performance degradation compared with what occurs at short z. The physical explanation of the trend of $P_{avg,Opt}$ described in the previous section (TRSF and EHS-DK fiber) is still applicable for this case (SSMF and EHS-DK fiber). When Tables 6.5 and 6.6 are compared at $z = 20$ km, $P_{avg,Opt}$ in the case of TRSF and EHS-DK fiber is higher than that for SSMF and EHS-DK fiber. Although SSMF is more linear than TRSF as explained earlier, its large dispersion

compared with TRSF results in a longer length of EHS-DK fiber being required. The longer length of EHS-DK fiber implies stronger nonlinear effects, which is undesirable. At short transmission distance z the performance degradation is mainly due to nonlinearity as explained in the previous section. Due to the longer length of EHS-DK fiber required and the fact that the transmission distance z is not sufficiently long to sufficiently disperse and attenuate the signal during the propagation in SSMF, $P_{avg,Opt}$ in this case (SSMF and EHS-DK fiber) is lower than $P_{avg,Opt}$ in the previous case (TRSF and EHS-DK fiber).

However, as the transmission distance z becomes longer, the loss and dispersion experienced by the signal during the propagation in SSMF are increased, which in effect reduces the effect of nonlinearity in the EHS-DK fiber. Since SSMF has larger dispersion than TRSF, pulses are dispersed more severely in SSMF. This combined with the fact that SSMF is more linear than TRSF allows higher $P_{avg,Opt}$ than TRSF at large z as shown in Table 6.6. However, when the system performance in terms of Q at a given z is considered, the benefit of less nonlinearity and larger dispersion in the transmission fiber in this case is offset by higher additional loss in the dispersion compensation process since longer length of EHS-DK fiber is required in this case. For a given transmission distance z, the length of EHS-DK fiber required in this case is approximately four times longer than what is needed when TRSF is employed as the transmission fiber. Consequently, for a given z (190 km for example), the values of Q for all modulation formats in this case are lower than those corresponding to the system employing TRSF as the transmission fiber. Moreover, the maximum transmission distance $z_{\max}$ when SSMF is employed as the transmission fiber is shorter than $z_{\max}$ corresponding to the case when TRSF is employed (see the bottom parts of Tables 6.5 and 6.6 for comparison).

6.5.2.2 Optimum Transmitter Filter Bandwidth

When the transmitter filter bandwidth BW_{Tx} is considered, the trends in BW_{Tx} for AMI and no PM for the case of SSMF are not similar to that for TRSF. Since the

dispersion value of SSMF is large, the effect of IFWM is more severe compared with the system employing TRSF. In fact, IFWM is the dominant nonlinear intrachannel impairment when the local dispersion is large. Note that IXPM is still present in this case. Unlike IXPM, the effect of IFWM increases with pulse overlap. Thus, for AMI small transmitter filter bandwidth BW_{Tx} is desirable at large z in this case to reduce the pulse spread, hence decreasing the adverse effect of IFWM. Although the effect of IXPM is increased at small BW_{Tx}, IFWM is still the dominant source of impairment at small BW_{Tx} due to large accumulated dispersion. In addition, the AMI property of alternate signs between adjacent pulses prevents initial overlaps between adjacent pulses caused by the filter, and indirectly reduces IXPM by mean of minimizing the effect of IFWM as discussed earlier. Consequently, small BW_{Tx} yields better performance than large BW_{Tx} for AMI at large z. It should be noted, however, that if the transmitter filter bandwidth is too small, the filter can cause intolerable waveform distortion. Hence, there exists an optimum BW_{Tx}, which is equal to 2 in this case.

Conversely, large BW_{Tx} yields better system performance in term of Q for AMI at small z when the transmission fiber is SSMF. At small z, the effects of IXPM and IFWM are comparable. This is due to the fact that the accumulated dispersion is not sufficiently large to cause the effect of IFWM to be dominant because the time during which pulses partially overlap is no longer negligible compared with the total propagation time. When the transmitter filter bandwidth BW_{Tx} is small, the effect of IXPM degrades the system performance more severely than IFWM at short z. Since the SSMF has large local dispersion, spreading pulses quickly to reduce the IXPM is more effective than reducing the overlap. Therefore, large signal bandwidth is beneficial at short z for AMI to reduce the effect of IXPM.

For no PM, it is found that the optimum transmitter filter bandwidth BW_{Tx} is always equal to 4 (no filtering at all) regardless of the transmission distance in this case. At short transmission distance z, large transmitter filter bandwidth BW_{Tx} yields better performance due to the same explanation given for AMI. However, large filter bandwidth is still advantageous for no PM at large z. This can be understood as follows. Unlike

AMI, adjacent pulses have identical sign in the case of no PM. This makes the no PM signal susceptible to waveform distortion caused by the filter at the transmitter. At small transmitter filter bandwidth BW_{Tx}, the waveform distortion caused by the filter results in initial overlaps between adjacent pulses in the case of no PM, which favor the nonlinear intrachannel impairments. Since the local dispersion of the transmission fiber is large, IFWM is severe even at small signal bandwidth. As discussed in the previous section, IFWM further enhances IXPM in the case of no PM signal. Thus, IFWM and IXPM, favored by initial pulse overlaps, considerably degrades the eye profile as well as the Q value at small filter bandwidth as shown in Fig. 6.14a which is the eye diagram for no PM at the transmission distance of 180 km when $BW_{Tx} = 2$, and $P_{avg,Opt} = 11$ dBm. The Q value for no PM at $BW_{Tx} = 2$ is only 12.8 dB, which is well below the threshold value of 15.6 dB. It is clearly seen that the eye profile of no PM signal suffers considerable effects of IXPM and IFWM at small filter bandwidth BW_{Tx}. The intrachannel IXPM results in severe timing jitter (pulse peaks are shifted away from the center of bit slots) whereas IFWM causes noticeable amplitude jitter and generation of ghost pulses. The generation of ghost pulses generally results in ISI in empty bit slots, which is clearly seen in Fig. 6.14a. Note that IXPM also causes ISI in empty bit slots. The IXPM shifts the pulse peaks, causing the pulse tails to reside in empty bit slots. In fact, the overlaps among pulse tails enhances the generation of ghost pulses.

The effects of intrachannel impairments are significantly reduced at large filter bandwidth as shown in Fig. 6.14b, which corresponds to $BW_{Tx} = 4$. At large BW_{Tx}, the filter-induced initial overlaps between pulses, which favor the nonlinear impairments, are negligible. Thus, both the effects of IXPM and IFWM are reduced significantly at large BW_{Tx}. Moreover, pulses spend short period of time partially overlapping due to strong effect of dispersion at large BW_{Tx}; hence, the effect of IXPM is further decreased. Short period of time during which pulses partially overlap also reduces the interaction between IXPM and IFWM, therefore reducing the enhancement of IXPM caused by IFWM. It should be noted, however, that the timing jitter due to IXPM is still observable when the bandwidth is large. Due to large accumulated dispersion and large signal bandwidth, the

dominant nonlinear intrachannel impairment is IFWM. The amplitude jitter and generation of ghost pulses in empty bit slots are the sources of performance degradation, which are clearly seen from Fig. 6.14b.

It should be noted that the effects of IXPM and IFWM are less for CWSW and AMI due to the fact that adjacent pulses have opposite signs for those signal formats, which will be discussed later. Similar to the system employing TRSF, the optimum transmitter filter bandwidth BW_{Tx} for CWSW is always equal to unity independent of the transmission distance z as listed in Table 6.6. This is simply because the pulse peak, which represents bit 1, decreases with the increase in BW_{Tx}. It should be noted, however, that narrow signal bandwidth provides an additional advantage in this case because it reduces the effect of IFWM, which is the dominant source of impairment for a system employing SSMF as a transmission fiber.

6.5.2.3 Performance Comparison

Compared with TRSF, SSMF requires longer length of EHS-DK fiber for dispersion compensation. This results in high loss in the dispersion compensation. Thus, the maximum transmission distances $z_{\max}$ for all modulation formats in this case are less than 200 km. Shown in Figs. 6.15a to 6.15c are the eye diagrams at optimum transmitted power $P_{avg,Opt}$ and transmitter filter bandwidth BW_{Tx} for CWSW, AMI and no PM, respectively, when the transmission distance is 184 km ($z_{\max}$ for CWSW). It is seen that the nonlinear intrachannel impairment that limits the system performance is IFWM although IXPM still exists. The eye profile for no PM suffers intense effect of IFWM, which causes severe amplitude jitter and generation of ghost pulses (ISI in empty bit slots representing bit 0's) as shown in Fig. 6.15c. Although IFWM is dominant, the timing jitter caused by IXPM is clearly seen. The intensity fluctuation caused by IFWM enhances IXPM in the case of no PM.

Compared with no PM, the eye profile for CWSW is significantly better as shown in Fig. 6.15a. This is due to the fact that the strength of IFWM depends on the phases of the interacting pulses. For CWSW, adjacent pulses have alternate signs, which in effect reduces the effect of IFWM as discussed in Chapter 3. The reduction of IFWM is clearly

seen when the eye profiles of CWSW and no PM are compared. The amplitude jitter in the case of CWSW is less than that present in the case of no PM. The reduction in IFWM also helps reduce the effect of IXPM. The eye profile of CWSW is more symmetric than that of no PM due to less effect of IXPM. When the eye diagram in the case of AMI signal format is considered (Fig. 6.15b), the eye opening is larger than those of CWSW and no PM. Similar to CWSW, adjacent pulses have opposite signs in the case of AMI. However, AMI also possesses an additional property in terms of relative signs among pulses. For CWSW, two consecutive pulses have the same sign when they are separated by an odd number of empty bit slots (bit 0's). Due to the encoding in the case of AMI, two consecutive pulses always have opposite sign regardless of the number of empty bit slots in between. This property in effect suppresses the generation of ghost pulses in empty bit slots due to IFWM as discussed in Chapter 3. It should be noted, however, that amplitude jitter still occurs but reduced, similar to CWSW.

The suppression of ghost-pulse generation allows higher transmitted power in the case of AMI. The optimum transmitted power $P_{avg,Opt}$ for AMI is 2 dB (≈ 1.6) higher than CWSW. Hence, the eye opening in the case of AMI is larger than that of CWSW, resulting in 1.2 dB better Q value. However, higher transmitted power means higher effect of nonlinearity. AMI experiences more intense effects of IFWM and IXPM than CWSW and no PM, resulting in more severe amplitude jitter and timing jitter. This is clearly seen when Fig. 6.15b is compared with Figs. 6.15a (CWSW) and 6.15c (no PM). This suggests that the advantage in allowing higher transmitted power compared with CWSW comes with poorer eye profile. Plotted in Fig. 6.15d is the eye diagram for AMI when the transmitted power is reduced to 11 dBm ($P_{avg,Opt}$ for CWSW). At the same transmitted power of 11 dBm, the eye profiles for both CWSW (Fig. 6.15a) and AMI (Fig. 6.15b) are comparable. The benefit of suppressing the ghost-pulse generation is barely observable. In terms of the Q value, AMI signal format performs better than CWSW by only 0.5 dB at the cost of encoding required in the signal generation at the transmitter. The CWSW signal format can achieve the maximum transmission distance of 204 km, which is only 4 km shorter than the maximum for AMI. It should be pointed out

that longer transmission distance in the case of AMI is due to its higher optimum transmitted power, which comes however with poorer eye profile at the receiver.

For the case considered here of SSMF, there is less difference between the eye profiles of the different systems (Fig. 6.15) than is the case for TRSF shown in Fig. 6.13. This is primarily due to the fact that the pulse-sign characteristics of CWSW and AMI are mainly for combating the effect of IFWM, which is the dominant intrachannel impairment when the local dispersion of the transmission fiber is large. Although the attenuation of the transmission fiber is 0.2 dB/km, the loss experienced by the signal is 0.24 dB per one-kilometer increase in the transmission distance z because of the additional loss due to the attenuation of the dispersion compensating fiber. In terms of the maximum transmission distance $z_{\max}$, the system employing SSMF as the transmission fiber performs poorer than the system employing TRSF with the same dispersion compensating fiber. This is mainly owing to the longer length of the dispersion compensating fiber required for SSMF given that the transmission distance z is the same for both systems. However, higher optimum transmitted power in this case suggests that if the loss associated with the dispersion-compensation process is reduced or eliminated, the maximum transmission distance in the system employing SSMF can be made longer than that corresponding to the system employing TRSF. This leads to another type of system in which the dispersion compensating fiber is deployed as a transmission fiber. For this fiber configuration, the loss associated with the dispersion compensation is counted as the transmission loss. This type of system is studied in the next section.

6.5.3 Large Local Dispersion with Dispersion Compensating Fiber employed as Transmission Fiber

In this section, the system in which the transmission span consists of two transmission fibers is studied. This system corresponds to curve (c) in Fig. 6.9. The first transmission fiber is still SSMF, and the second transmission fiber is a reverse-dispersion fiber (RDF). The characteristic of the SSMF is the same as that used in the previous section. The RDF has a dispersion of –26.91 ps/(km·nm), a nonlinear refractive index of 2.3×10^{-20} m^2/W, an effective core area of 25 μm^2, and a loss of 0.22 dB/km. The ratio

between the absolute dispersions of SSMF and RDF is approximately 1.6; thus, the length of SSMF is 1.6 time longer than the length of RDF for a given normalized transmission distance z.

Listed in Table 6.7 are the Q values at different transmission distances (the length of SSMF plus the length of RDF), and corresponding optimum system parameters for CWSW, AMI and no PM. Also listed at the bottom are the maximum transmission distances and corresponding optimum system parameters. When Table 6.7 and Table 6.6 are compared, it is seen that the values of Q listed in Table 6.7 are higher than those in Table 6.6 for all transmission distances z except for $z = 20$ km. The higher values of Q can be understood from the fact that in this case the dispersion compensation is performed by the second transmission fiber; hence, the loss due to dispersion compensation is counted as transmission loss. Note that the total transmission distance z in this case is the length of SSMF and RDF combined whereas the total transmission distance z in the system employing SSMF and EHS-DK fiber, discussed in the previous section, is the length of SSMF only. At short transmission distance z, 20 km for example, the length of SSMF is only 12.26 km in this case. The attenuation and accumulated dispersion in SSMF, deployed as the first transmission fiber, are not sufficient to attenuate and disperse the signal so that its intensity at the input to RDF is considerably greater than the input to the EHS-DK fiber in the previous case. Thus, the optimum transmitted powers $P_{avg,Opt}$ for all signal formats in this case are less than those listed in Table 6.6 at $z = 20$ km to avoid severe effects of nonlinearity in the RDF. This results in lower values of Q at $z = 20$ km in this case compared with the system employing SSMF and EHS-DK fiber.

It should be noted that the RDF has a smaller nonlinear refractive index and a larger effective core area than the EHS-DK fiber resulting in smaller nonlinearities. This is advantageous because nonlinearity reduces the effectiveness of dispersion compensation. As a result, the optimum transmitted power $P_{avg,Opt}$ starts to increase with z at shorter z compared with the system employing SSMF and EHS-DK fiber. It is seen from Tables 6.6 and 6.7 that the optimum bandwidths BW_{Tx} are independent of whether EHS-DK fiber or RDF is used for compensation. This is because the main transmission

fiber is SSMF in both cases. The significant advantage of employing RDF is that it yields longer transmission distance. Utilizing RDF allows more than 30 km increases in the maximum transmission distances $z_{\max}$ for all modulation formats compared with the system employing EHS-DK fiber at the same optimum system parameters. CWSW and AMI help increase the maximum transmission distances by 5 km and 10 km, respectively, compared with no PM as listed at the bottom part of Table 6.7.

Plotted in Fig. 6.16 are the eye diagrams for CWSW, AMI, and no PM at corresponding optimum system parameters when $z = 216$ km, which is the maximum transmission distance for CWSW. The eye diagrams shown in Fig. 6.16 are similar to those shown in Figs. 6.15a to 6.15c although the transmission distance corresponding to Fig. 6.16 is 32 km longer. The similarity is primarily due to the fact that the main transmission fiber in both cases is SSMF. The dominant nonlinear intrachannel impairment is still IFWM, causing amplitude jitter and generation of ghost pulses. The optimum transmitted power for AMI is still 2 dB higher than CWSW, providing 1.1 dB better Q compared with CWSW. Similar to the results discussed in the previous section, the advantage of allowing higher transmitted power in the case of AMI is negated by more severe effects of IFWM and IXPM. Shown in Fig. 6.17 are the close-up looks of the eye diagrams for CWSW and AMI at the same transmission distance ($z = 216$ km) and optimum BW_{Tx} as those in Fig. 6.16. However, the transmitted power P_{avg} corresponding to Fig. 6.17 is 11 dB for both CWSW and AMI. It is seen that the eye profiles for CWSW and AMI are nearly identical. The AMI signal format experiences slightly less effect of IFWM compared with CWSW in terms of amplitude jitter and ISI in empty bit slots. The AMI signal format has 0.5 dB better Q value than CWSW, whose Q value is 15.7 dB at $z = 216$ km. This seems to indicate that the benefit of having opposite signs between adjacent pulses regardless of the number of empty bit slots in between does not provide any significant advantage unless the effect of nonlinearity is strong where it allows 2 dB higher transmitter power resulting in 5 km longer transmission distance.

For all systems investigated in this section, it is seen that dispersion compensation is a powerful method for combating the effect of dispersion. Still, nonlinearity prevents the perfect compensation. In terms of maximum transmission distance $z_{\max}$, the

combination of SSMF and RDF performs the best due to the fact that RDF functions as both the dispersion compensating fiber and a transmission fiber. On the other hand, the system employing SSMF as the transmission fiber and EHS-DK fiber as the dispersion compensating fiber allows the shortest maximum transmission distance. This is mainly because SSMF has large local dispersion; hence, a long length of EHS-DK fiber is required, which in effect introduces intolerable loss. For all types of fiber configurations investigated, the fiber attenuation and nonlinearity are the limiting factors, preventing the transmission to be longer than approximately 200 km. In order to increase the transmission distance, in-line optical amplifiers are necessary to periodically compensate for the fiber loss along the transmission link. In the next section, multiple-span systems employing in-line optical amplifiers to increase the total transmission distance are investigated. However, the system employing SSMF and EHS-DK fiber is not investigated further in the next section since the results presented in this section indicate that that system performs poorest among the three types of systems considered.

6.6 MULTIPLE-SPAN DISPERSION-MANAGED SYSTEM EMPLOYING IN-LINE OPTICAL AMPLIFIERS AND OPTICAL PREAMPLIFIER

In this section, multiple-span dispersion-managed systems employing in-line optical amplifiers as well as optical preamplifiers are studied. In these systems, the fiber loss and accumulated dispersion are periodically compensated along the transmission link. Although large amplifier spacing is preferable to save component costs, large amplifier spacing implies large ASE noise introduced to the system by the amplifier. This is because the power of ASE noise is proportional to the amplifier gain, which has to be increased with the increase in the amplifier spacing to compensate for the attenuation. Additionally, large transmitted power as well as large signal power at a repeater output is required when the amplifier spacing is large in order to sufficiently compensate for the fiber loss. Since an optical fiber is not a linear medium, high signal power results in severe effects of nonlinearity. Thus, shorter amplifier spacing generally allows longer total transmission distance. Although the dispersion accumulated along the transmission

link can be totally compensated at the receiver, this approach is not practical in some circumstances. This is because as the number of spans increases, the accumulated dispersion can be so large that the loss associated with the dispersion compensation process is intolerably severe. Moreover, the long length of the dispersion compensating fiber requires large space at the receiver site, which can cause some problems in terms of practical implementation. Consequently, in this investigation the accumulated dispersion is periodically compensated along the transmission link with the period equal to the amplifier spacing. The amplifier spacings of 160 km and 120 km are investigated for comparison. Note that the amplifier spacing of 160 km is comparable to the maximum transmission distance that can be achieved in the case of single span (around 200 km). The system, employing TRSF as the transmission fiber and EHS-DK fiber as the dispersion compensating fiber, will be investigated first.

6.6.1 Moderate Local Dispersion with Modular Dispersion Compensating Fiber

In this system, the transmission fiber for each span is TRSF. Dispersion compensation is performed at the input of each in-line optical amplifier, and at the input of the optical preamplifier at the receiver (see Fig. 2.7b) to periodically return the accumulated dispersion to zero. The dispersion compensating fiber is still EHS-DK fiber, whose length is tailored so that the accumulated dispersion in each span is returned to zero. Listed in Table 6.8 are the system performance in terms of Q and optimum system parameters as a function of the number of spans for the system deploying TRSF as the transmission fiber when the amplifier spacing is 160 km. It is clearly seen that for all modulation formats the optimum transmitted power $P_{avg,Opt}$ and the Q values decrease with the increase in the number of spans. The decrease in $P_{avg,Opt}$ with the increase in the number of spans can be understood from the fact that as the number of spans increases, the effects of nonlinearity accumulate. In order to reduce the effects of nonlinearity, the transmitted power has to be decreased. The accumulation of the nonlinear effects and ASE noise output from the in-line optical amplifiers are the major factors that cause Q to decrease as the number of spans increases.

The larger the number of spans, the more linear the optical fiber has to be. It should be noted that when the transmitter filter bandwidth BW_{Tx} is considered, its optimum values do not change with the number of spans. Since the local dispersion of the transmission fiber (TRSF) is moderate, the dominant nonlinear intrachannel impairment is IXPM similar to the case of single-link system. In order to reduce the effect of IXPM, pulses have to spread as quickly as possible. Thus, the optimum BW_{Tx} is equal to 4 for AMI and no PM to maximally spread the pulses since the effect of dispersion is proportional to signal bandwidth. As explained earlier, the optimum BW_{Tx} for CWSW is unity in order to maximize the pulse peak, which represents the signal level for bit 1.

In terms of Q, CWSW and AMI perform better than no PM by 1 dB and 1.5 dB, respectively, at all number of spans. For CWSW and AMI, the accumulated nonlinearity and ASE noise limit the maximum transmission distance to 480 km, which corresponds to three spans. At that distance, the Q value for CWSW is 16.0 dB, which is 0.5 dB lower than that for AMI. It should be noted that the optimum transmitted power $P_{avg,Opt}$ in the case of AMI signal format is 6 dBm, which is 1 dB higher than that of CWSW. Plotted in Fig. 6.18 are the eye diagrams for CWSW, AMI and no PM at the optimum system parameters listed in Table 6.8 when the total number of spans is 3. For no PM, the signal suffers severe timing jitter as shown in Fig. 6.18c similar to the single-span case. The eye profiles for CWSW and AMI, shown in Figs. 6.18a and 6.18b, respectively, are significantly better than no PM. The effect of IXPM that causes timing jitter is reduced considerably in the case of CWSW and AMI. Although the AMI signal format allows higher optimum transmitted power $P_{avg,Opt}$ by 1 dB compared with CWSW, the effect of IXPM is more severe in the case of AMI, resulting in only 0.5 dB better Q than CWSW.

Unlike a linear system, the increase in the transmitted power above the optimum does not result in an increase in the Q value. At the transmitted power of 6 dBm and $BW_{Tx} = 1$, the Q value in the case of CWSW is reduced by 0.08 dB compared with the Q value at the optimum transmitted power of 5 dBm. The reduction in the Q value is due to severe effect of nonlinearity at high signal power. Plotted in Fig. 6.19 are the eye diagrams for CWSW and AMI at the optimum transmitted power for CWSW ($P_{avg,Opt} = 5$

dBm). Note that the optimum filter bandwidth for AMI is still equal to 4. It is seen that the eye profiles for both CWSW and AMI are nearly identical. The eye opening for AMI is slightly larger than that for CWSW, resulting in 0.4 dB better system performance in terms of the Q value. The amplifier spacing of 160 km allows the total transmission distance to be about 2.5 times longer than that corresponding to the case of a single span. In order to extend the total transmission distance further, the amplifier spacing has to be reduced.

The Q values and corresponding optimum system parameters as a function of the number of spans when the amplifier spacing is reduced to 120 km are listed in Table 6.9. Similar to the case when the amplifier spacing is 160 km, the values of Q and the optimum transmitted power $P_{avg,Opt}$ for all considered modulation formats decrease with the increase in the number of spans. The optimum transmitter filter bandwidth BW_{Tx} for AMI and no PM is still equal to 4 and regardless of the number of spans. For CWSW, the optimum transmitter filter bandwidth is unity as expected. Decreasing the amplifier spacing from 160 km to 120 km allows the total transmission distance to extend from 480 km to 960 km (8 spans) in the case of the CWSW and AMI signal formats. That transmission distance is approximately four times longer than the maximum transmission distance that can be achieved in the single-span system. At such a transmisssion distance, the Q values for CWSW and AMI are 16.0 dB and 16.4 dB, respectively. Compared with the no PM signal format, CWSW and AMI yield better system performance by 0.9 dB and 1.3 dB, respectively.

Plotted in Fig. 6.20 are the decreases in Q, relative to their values for $M = 1$, as a function of the number of spans M, for all modulation formats. Note that the dotted curve in Fig. 6.20 is the prediction of the Q degradation by considering only the degradation due to the accumulated ASE noise and neglecting the nonlinear effects in the subsequent spans. The purpose of considering this case is to be able to see the extent to which nonlinearity degrades system performance beyond that of the ASE noise. The case where nonlinearity is neglected in subsequent spans may be evaluated semi-analytically as follows. When the transmission fiber is linear, and the gain of an in-line amplifier exactly compensates for the corresponding span loss, the eye opening in (6.11) is

independent of the number of spans for a given transmitted power. However, the denominator in (6.11) increases with the number of spans due to the increase in the accumulated ASE noise at the receiver. It is seen from (6.38) and (6.39) that the variances of the signal-spontaneous beat noise increase linearly with the number of spans. On the other hand, the variance of the spontaneous-spontaneous beat noise increases quadratically with the number of spans as seen from (6.40). By using the assumption that the subsequent spans following the first span is linear, the degradation in the Q values due to the accumulation of the ASE noise for a multiple-span optical-preamplifier system can be semi-analytically calculated from

$$\Delta Q = 20\log_{10}\left(\frac{\sqrt{\sigma_{q-sp,1}^2+\sigma_{sp-sp}^2}+\sqrt{\sigma_{q-sp,0}^2+\sigma_{sp-sp}^2}}{\sqrt{M\sigma_{q-sp,1}^2+M^2\sigma_{sp-sp}^2}+\sqrt{M\sigma_{q-sp,0}^2+M^2\sigma_{sp-sp}^2}}\right), \qquad (6.43)$$

where σ_{sp-sp}^2 is the variance of the spontaneous-spontaneous beat noise, and $\sigma_{q-sp,1}^2$ and $\sigma_{q-sp,0}^2$ are the variances of the signal-spontaneous beat noise for bit 1 and bit 0, respectively, all of which are obtained from the simulation when only the first span is considered. It is found that the difference in ΔQ evaluated by using (6.43) for all modulation formats is negligibly small. Therefore, the prediction of ΔQ with respect to the first span in the case of the CWSW signal format is chosen as a representative for comparison with the performance degradations in terms of Q obtained from the numerical simulation. When the predicted ΔQ calculated from (6.43) is considered (the dotted curve), ΔQ decreases by 3 dB for each doubling of the number of spans. For example, ΔQ at 2 spans is 3 dB less than that at 1 span. This indicates that the dominant noise at the receiver is the signal-spontaneous beat noise because (6.43) reduces to $\Delta Q \approx 20\log_{10}\left(1/\sqrt{M}\right)$ when the spontaneous-spontaneous beat noise is negligible compared with the signal-spontaneous beat noise.

The deviation of the performance degradation for all modulation formats from the degradation caused by the accumulation of ASE noise is mainly due to the accumulated effects of nonlinearity, which increase with the number of spans. Decreasing the transmitted power reduces the fiber nonlinearity. However, the effects of nonlinearity still

accumulate along the transmission link, thus decreasing the system performance. In fact, the degradation rates for all modulation formats are approximately twice faster than the degradation rate due to the accumulated ASE noise alone. Large deviation indicates that the effects of accumulated nonlinearity along the transmission link are strong. The degradation rate for no PM tends to be slightly less than the other signal formats. This is due to the fact that the first span is used as the reference point, and that the optimum transmitted power at the first span for no PM is lower than those of the CWSW and AMI signal formats; hence, no PM induces lowest fiber nonlinearity. Although the degradation rates for CWSW and AMI are higher than that of no PM, the CWSW and AMI signal formats still perform better than no PM at all number of spans considered since CWSW and AMI are more resistant to IFWM than no PM is, which helps reduce the effect of IXPM as explained earlier.

Fig. 6.21 is the plot of eye diagrams at corresponding optimum system parameters listed in Table 6.9 when the total number of spans is 8 (total transmission distance of 960 km). As expected, the effect of IXPM is significant, resulting in noticeable timing jitter. The no PM signal (Fig. 6.21c) suffers the most severe effect of IXPM compared with CWSW and AMI due to the enhancement of IXPM by IFWM. Reducing the effect of IFWM helps decrease the effect of IXPM considerably in the case of the CWSW and AMI signal formats as shown in Figs. 6.21a and 6.21b, respectively. The eye profiles for CWSW and AMI are nearly identical. Because the effect of IFWM is not severe compared with IXPM when the local dispersion is not large, AMI performs better than CWSW by only 0.4 dB in terms of Q resulting from AMI having slightly larger eye opening than CWSW. The slight improvement is achieved at the cost of encoding circuit at the transmitter. The advantage of AMI over CWSW in terms of minimizing the ISI on empty bit slots by suppressing the generation of ghost pulses caused by IFWM is not apparent in this case. It should be noted, however, that when the local dispersion of the transmission fiber is large, the dominant intrachannel impairment is IFWM due to severe pulse overlaps. In addition, in multiple-span systems the effects of nonlinearity are accumulated along the transmission path although the dispersion is periodically compensated. Therefore, suppressing the generation of ghost pulses could play an important role in improving system performance of the multiple-span system employing

the optical fiber having large dispersion. The performance of such a system is investigated in the next section.

6.6.2 Large Local Dispersion with Dispersion Compensating Fiber employed as Transmission Fiber

In this system, the dispersion compensation is not periodically performed at the input of each in-line optical amplifier and at the input to the optical preamplifier. Instead, the dispersion compensation is periodically performed within the transmission span. Each span consists of SSMF and RDF. The role of the RDF is to serve both as a transmission fiber and the dispersion compensating fiber. Similar to the case of a single-span system, the lengths of SSMF and RDF are adjusted so that the accumulated dispersion returns to zero at the span output. The system performance in terms of Q and corresponding optimum system parameters as a function of the number of spans are listed in Table 6.10. Similar to the multiple-span system employing TRSF, the optimum transmitted power $P_{avg,Opt}$ and Q for all modulation formats decreases with the increase in the number of spans. When Table 6.10 is compared with Table 6.8, the optimum transmitted power $P_{avg,Opt}$ and Q in this case is higher at all number of spans. This is due to the fact that SSMF is more linear than TRSF and that the dispersion compensation is performed by the second transmission fiber. At the transmission distance of 640 km, which corresponds to 4 spans, the Q value for CWSW is only 0.2 dB below the threshold value of 15.6 dB. In the previous case where the transmission fiber is TRSF, the Q value for CWSW is 2.4 below the threshold at the same transmission distance. This indicates that the combination of SSMF and RDF can yield longer transmission distance than TRSF and EHS-DK fiber at the same span length.

By sufficiently reducing the span length to be below the maximum transmission distance that can be achieved in the case of single span, the total transmission distance can be increased significantly for multiple-span systems. Large transmission distance implies severe accumulated nonlinear effects. Since the main transmission fiber is SSMF whose dispersion is large, the dominant nonlinear impairment is IFWM. At large transmission distance, the advantage of AMI over CWSW in terms of combating the

effect of IFWM on empty bit slots starts to significantly help improve the system performance. For AMI, the Q value is 16.9 dB at 640 km. This value of Q is 1.5 dB better than that of CWSW. Suppressing the generation of ghost pulses in empty bit slots allows the optimum transmitted power $P_{avg,Opt}$ for AMI to be higher than CWSW by 3 dB.

The eye diagrams at corresponding optimum system parameters listed in Table 6.10 when the total number of spans is 4 (640 km of total transmission distance) are plotted in Fig. 6.22. Similar to the single-span case, the effects of IFWM as well as IXPM are strong in the case of no PM, causing the Q value to be only 14.4 dB at the optimum system parameters. Strong nonlinear impairments result in severe amplitude jitter and timing jitter as seen in Fig. 6.22c. Alternate signs between adjacent pulses in the case of CWSW help improve the system performance by 1 dB compared with no PM. Moreover, the eye profile for CWSW (Fig. 6.22a) is better than that for no PM. Due to the fact that the optimum transmitted power for AMI is 3 dB higher than CWSW, the amplitude jitter and timing jitter are more severe in the case of AMI signal format as seen in Fig. 6.22b. Still, the Q value for AMI is 1.5 dB and 2.5 dB larger than CWSW and no PM, respectively. The eye diagrams for CWSW and AMI at the same transmitted power of 5 dBm (optimum for CWSW) are plotted in Figs. 6.23a and 6.23b, respectively. It is seen that the eye profiles for both signal formats are similar except that the eye opening for AMI is wider than CWSW, resulting in AMI having 0.6 dB larger Q than CWSW. This is mainly due to the fact that AMI is more robust to the effect of IFWM than CWSW by means of suppressing the ghost-pulse generation.

In order to gain further understanding on the accumulated effect of nonlinearity, simulations are conducted for systems in which the amplifier spacing is reduced to 120 km. The transmission fibers are still SSMF and RDF. Shorter amplifier spacing allows longer total transmission distance. At such a large transmission distance, the accumulated nonlinear impairments are expected to be more severe than those at short distance. The Q values and corresponding optimum system parameters as a function of the number of spans are listed in Table 6.11. It is seen that the values of Q and the optimum transmitted power $P_{avg,Opt}$ for all modulation formats still decrease with the increase in the number of

spans. Similar to the single-link case, the optimum BW_{Tx} for AMI and no PM are 2 and 4, respectively, and they are independent of the number of spans. For CWSW, the optimum BW_{Tx} is unity to maximize pulse peak and it is independent of the number of spans.

It is clearly seen that when the amplifier spacing is reduced from 160 km to 120 km, the total transmission distances for all modulation formats are increased dramatically. For CWSW and AMI, the maximum transmission distances are 1080 km and 1320 km, respectively, while it is 960 km for no PM. It should be noted that at the transmission distance of 1200 km, the Q value for CWSW is just 0.3 dB below the threshold. Similar to the case of 160-km amplifier spacing, the optimum transmitted power $P_{avg,Opt}$ for AMI is highest, permitting longer transmission distance and higher Q. Shown in Fig. 6.24 are the performance degradations in terms of Q with respect to the values at the first span for all modulation formats. Also shown in Fig. 6.24 is the prediction of the performance degradation due to the accumulated ASE noise alone, which is calculated from (6.43). Similar to the case of TRSF, the difference in performance degradations due to the accumulated ASE noise alone among all modulation formats is negligible. Therefore, the performance degradation due to the accumulated ASE noise alone in the case of the CWSW signal format is used as a representative case. The performance degradations as a function of the number of spans with SSMF (Fig. 6.24) are nearly identical to those for TRSF (Fig. 6.20). However, SSMF and RDF allow longer total transmission distance than TRSF and EHS-DK fiber at the same amplifier spacing. The severe effects of accumulated nonlinearity cause significant deviation of performance degradation from the degradation caused by the accumulated ASE noise alone, similar to the case of TRSF (Fig. 6.20). Due to the fact that IFWM is dominant in this case, the difference in the degradation rates between AMI and the other signal formats is noticeable. This is owing to the property of suppressing the ghost-pulse generation possessed by the AMI signal format. This benefit becomes more significant as the number of spans increases. Similar to the case of TRSF, the system performances of the CWSW and no PM signal formats degrade at nearly the same rate. Nevertheless, the CWSW signal format still performs better than no PM by approximately 1 dB at all

number of spans considered due to the fact that CWSW is more robust to the effect of IFWM than no PM.

The eye diagrams at the corresponding optimum system parameters listed in Table 6.11 when the total number of spans is 10 (1200 km of total transmission distance) are plotted in Fig. 6.25. At this large transmission distance, the generation of ghost pulses due to IFWM is apparent in the case of CWSW and no PM. The generation of ghost pulses in effect results in the ISI in empty bit slots, hence raising signal level for bit 0 as shown in Figs. 6.25a and 6.25c, which correspond to CWSW and no PM, respectively. Nevertheless, alternate signs between adjacent pulses in the CWSW signal still help improve the Q value by 1 dB as well as the eye profile by reducing the effect of IFWM. The eye profile for CWSW is still in better shape than that for no PM. For AMI, it has largest eye opening as seen in Fig. 6.25b; however, the eye has more severe amplitude jitter and the timing jitter than those of the other modulation formats due to its higher optimum transmitted power. Suppressing the generation of ghost pulses is evident in the case of AMI. The highest signal level for bit 0 in the case of AMI signal format is lower than that for CWSW and no PM.

The higher allowable transmitted power in the case of AMI results in the Q value of 16.9 dB, which is 1.6 dB higher than that of CWSW. For the comparison between CWSW and AMI, the eye diagrams for both signal formats when $P_{avg,Opt} = 1$ dBm (optimum for CWSW) are plotted in Fig. 6.26. When Fig. 6.26b is compared with Fig. 6.25b, it is clearly seen that the severe effects of nonlinearity are reduced significantly by decreasing the transmitted power. At the same transmitted power of 1 dBm, AMI performs better than CWSW by 0.8 dB in terms of the Q value, which in mainly due to the suppression of ghost pulses. This is clearly seen when the floor of the eye diagrams shown in Figs. 6.26a and 6.26b are compared. Suppressing the ghost pulses in the case of AMI significantly decreases ISI in empty bit slots as seen from Fig. 6.26b.

6.7 EFFECT OF FILTER AT FIBER INPUT ON SYSTEM PERFORMANCE OF CWSW SIGNAL FORMAT

One may notice that the locations of the optical filter at the transmitter for CWSW and AMI are different (see Figure 6.3). In the case of the CWSW signal format, there is no optical filter at the fiber input. In WDM systems employing DSF, the channel spacing has to be relatively large compared with the channel bandwidth to avoid the nonlinear interchannel impairments, which are significant when the dispersion of the transmission fiber is not large. When the channel spacing is sufficiently large, large signal bandwidth is allowed, which favors the CWSW signal format as suggested by the results discussed in Section 6.4. In WDM systems, a WDM multiplexer is generally placed at the fiber input to combine the different wavelengths together. In terms of the effect on a single channel, the WDM multiplexer can be modeled as an optical bandpass filter. Since the channel spacing is large in WDM systems employing DSF as the transmission fiber, the effect of the multiplexer on the signal can be neglected.

However, for dispersion-managed WDM systems, a fiber having large dispersion compared with DSF is deliberately chosen as the transmission fiber to allow narrow channel spacing. In these systems, the effect of the WDM multiplexer may no longer be negligible due to the fact that the channel spacing is now small. It should be noted that for AMI and no PM the effect of the WDM multiplexer modeled as an optical bandpass filter is already included by means of the bandwidth of the transmitter filter at the fiber input (see Fig. 6.3b). However, in the case of the CWSW signal format, the effect of the WDM multiplexer in dispersion-managed systems has not yet been investigated. To be consistent with the AMI and no PM signal formats, the multiplexer placed at the fiber input is modeled as a fifth order Butterworth filter. Its bandpass bandwidth is denoted by BW_{Mux} to avoid confusion with the bandwidth of optical filter used for generating the CWSW pulse train (see Fig. 6.3a). As suggested by the results discussed in Section 6.6, the optimum transmitter filter bandwidth is independent of the number of spans; thus, a single-span dispersion-managed system is investigated.

6.7.1 System employing TRSF and EHS-DK Fiber

For the single-span system employing TRSF as the transmission fiber and EHS-DK fiber as a dispersion compensating fiber, the optimum transmitter filter bandwidth BW_{Tx} for CWSW is unity regardless of the transmission distance. Listed in Table 6.12 is the system performance in terms of Q for CWSW as a function of the multiplexer bandwidth when $BW_{Tx} = 1$ and the transmission distance is 200 km. Since the dominant nonlinear intrachannel impairment in this system is IXPM, large signal bandwidth is preferable. As seen from Table 6.12, the Q value increases with the multiplexer bandwidth BW_{Mux}. At small BW_{Mux}, the multiplexer causes severe waveform distortion, which results in isolated pulses being broadened severely. The initial pulse spread combined with the small signal bandwidth in effect favors IXPM. Hence, the optimum transmitted power $P_{avg,Opt}$ when $BW_{Mux} = 1$ is lower that those at larger BW_{Tx} as listed in Table 6.12. Since the optimum BW_{Tx} is unity, the signal bandwidth at the multiplexer input is small. Therefore, when BW_{Mux} is sufficiently large, the multiplexer has no effect on the signal. In this case, the Q value reaches the value that corresponds to the case of no WDM multiplexer when $BW_{Mux} = 2.5$. This is beneficial because in WDM systems, narrow bandwidth implies that WDM channels can be packed effectively. Recall that the optimum bandwidth of the filter at the fiber input in the case of AMI and no PM is 4. Thus, CWSW has a bandwidth advantage compared with AMI and no PM in the system employing TRSF and EHS-DK fiber.

6.7.2 System Employing SSMF and RDF

For the system employing SSMF and RDF as the transmission fiber, IFWM is the dominant nonlinear intrachannel impairment. Since the effect of IFWM increases with pulse overlap, small signal bandwidth is preferable to reduce pulse spread. Table 6.13 lists the Q values at different BW_{Mux} when $BW_{Tx} = 1$ and the transmission distance is 210 km. At large multiplexer bandwidth, the system performance is similar to that corresponding to the case of no multiplexer at the fiber input. It is seen that there exists an optimum BW_{Mux} in this case. Similar to the previous case, the signal suffers severe

waveform distortion at small BW_{Mux}, which leads to severe nonlinear effects. However, the multiplexer can help decrease the signal bandwidth, which is desirable in this case because IFWM increases with the signal bandwidth. The Q value is improved by 0.2 dB when $BW_{Mux} = 2$ compared with the case of no multiplexer ($BW_{Mux} = 4$).

Shown in Fig. 6.27 are the eye diagrams for the CWSW signal at $BW_{Mux} = 2$ and $BW_{Mux} = 4$. When Figs. 6.27a and 6.27b are compared, it is clearly seen that the multiplexer helps reduce the amplitude jitter when $BW_{Mux} = 2$, resulting in better eye opening and better Q compared with the case of no multiplexer ($BW_{Mux} = 4$).

From the results discussed in this section, it can be concluded that the filter at the fiber input, which represents the WDM multiplexer, does not degrade the system performance of the CWSW signal format provided that the filter bandwidth is not too narrow. In the system employing TRSF and EHS-DK, the trend of the filter bandwidth at the fiber input for the CWSW signal format is similar to AMI and no PM. However, the filter at the fiber input does not yield any performance improvement for CWSW in this case. On the other hand, for the case where SSMF is the primary transmission fiber, the filter at the fiber input helps improve the system performance of CWSW signal format by decreasing the effect of IFWM.

6.8 SUMMARY

In this chapter, the performance improvements obtained from various modulation formats are compared in terms of the Q value and the eye profile. For the system employing DSF, it is found that CWSW significantly outperforms the other modulation formats due to PIE and spurious pulse suppression. For 40Gb/s single-span system employing an optical preamplifier, the maximum transmission distances that can be achieved by employing the CWSW signal format are 195 km when $D = +0.5$ ps/(km·nm) and 162 km when $D = -0.5$ ps/(km·nm). On the other hand, for AMI the maximum transmission distances are 187 km and 159 km when $D = +0.5$ ps/(km·nm) and $D = -0.5$ ps/(km·nm), respectively. For the dispersion-managed systems, the system performance for both CWSW and AMI are comparable over the broad ranges of parameters

considered. In the single-span dispersion-managed system employing TRSF and EHS-DK fiber, the maximum transmission distance in the case of CWSW signal format is 206 km while the AMI signal can achieve the maximum transmission distance of 208 km. However, CWSW has narrower bandwidth than AMI, which is advantageous in a WDM system. The dominant nonlinear intrachannel impairment in this case is IXPM. Due to the long length of EHS-DK fiber required, the maximum transmission distance that can be achieved from the CWSW signal format reduces to 184 km for the system employing SSMF and EHS-DK fiber. In the same system, the AMI signal format yields the maximum transmission distance of 188 km. Similar to the previous case, CWSW has a bandwidth advantage compared with AMI. For all transmission formats the transmission distance can be extended significantly when the dispersion compensation is performed within the transmission link. The system then employs two transmission fibers: SSMF and RDF. In such a system, the maximum transmission distance in the case of CWSW is 216 km and 221 km in the case of AMI. Due to the encoding at the transmitter, AMI is more effective than CWSW in combating the generation of ghost pulses caused by IFWM, which is the dominant nonlinear intrachannel impairment in the system employing SSMF. For multiple-span systems employing in-line optical amplifiers and preamplifier, the maximum transmission distance is 1080 km for CWSW and 1320 km for AMI when the amplifier spacing is 120 km. Although AMI performs better than CWSW when IFWM is dominant, AMI requires the encoder at the transmitter, and larger transmitter filter bandwidth than CWSW.

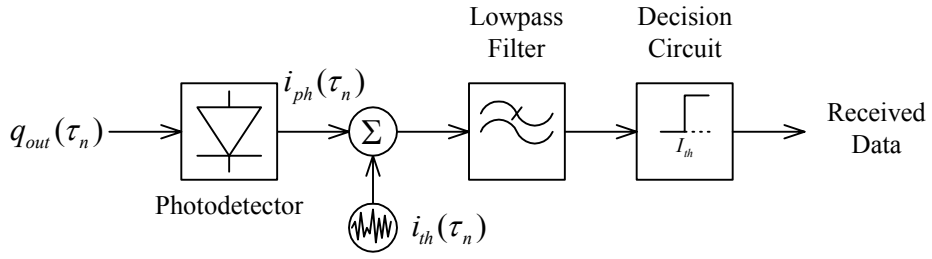

Fig. 6.1: Schematic diagram of the receiver.

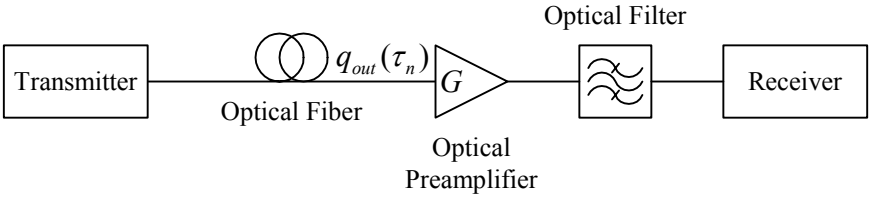

(a)

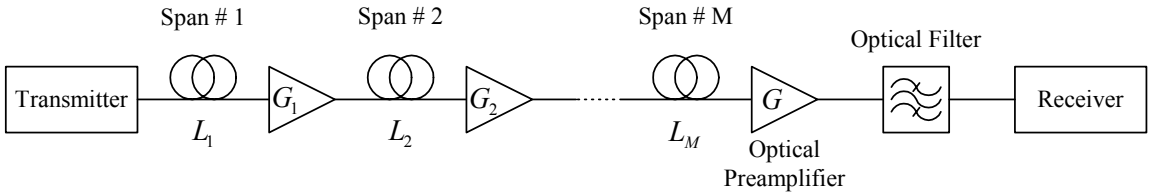

(b)

Fig. 6.2: Schematic diagrams of optical fiber communication systems. (a) Single-span system with optical preamplifier. (b) Multiple-span system with in-line optical amplifiers and optical preamplifier.

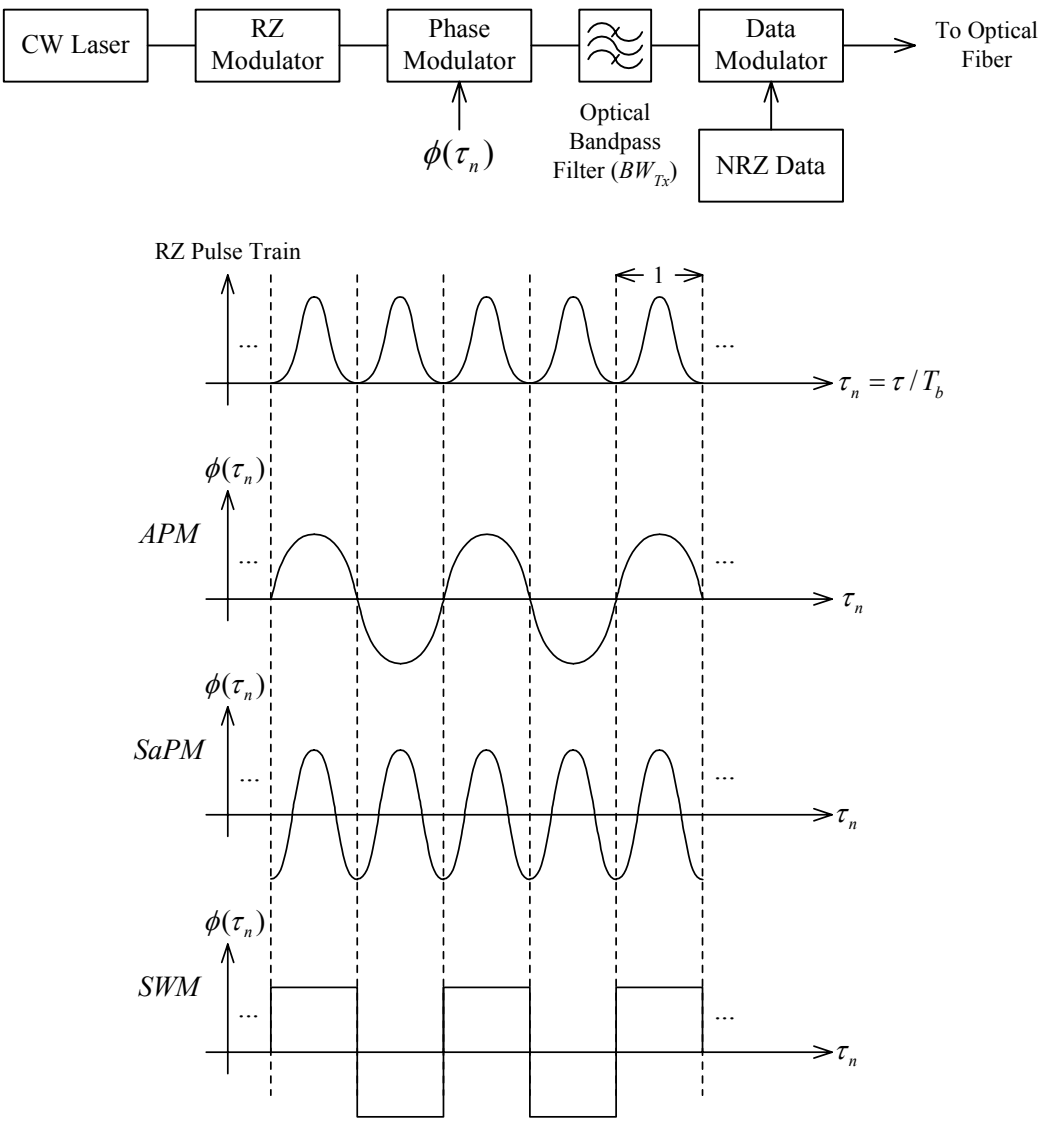

(a)

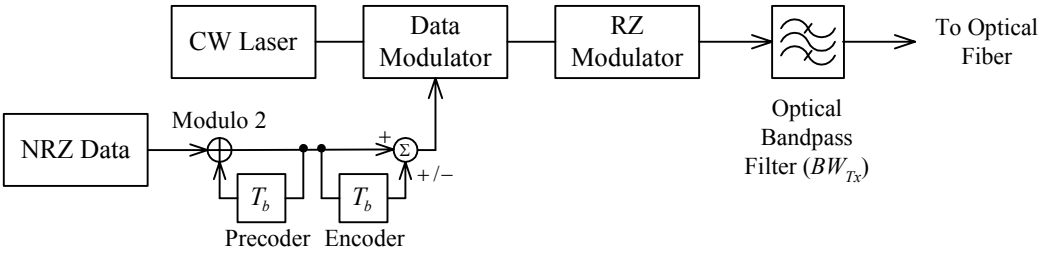

(b)

Fig. 6.3: Transmitter configurations. (a) APM, SaPM, SWM, and CWSW signal formats. (b) Optical duobinary, and AMI signal formats.

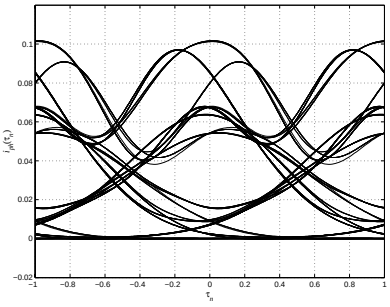

(a) APM ($B_{Opt} = 1.2$) : $Q = 16.0$ dB

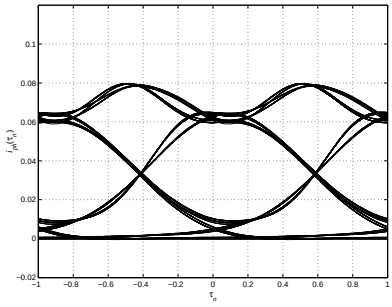

(a) SaPM ($B_{Opt} = -1.2$) : $Q = 18.3$ dB

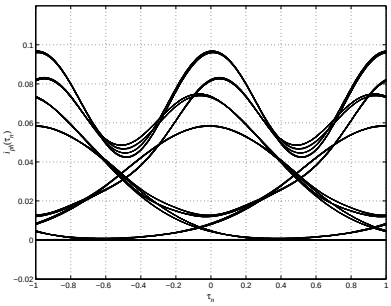

(c) SWM : $Q = 17.6$ dB

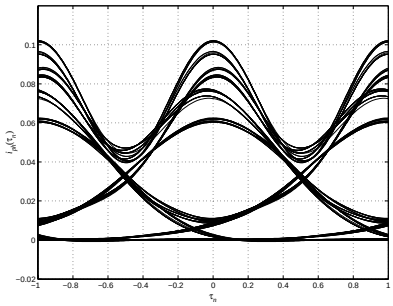

(d) CWSW : $Q = 18.3$ dB

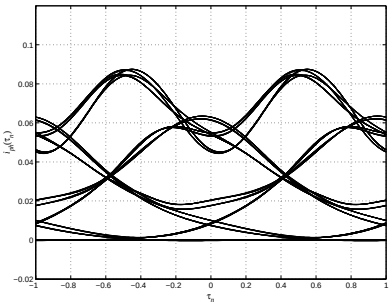

(e) Optical Duobinary : $Q = 12.2$ dB

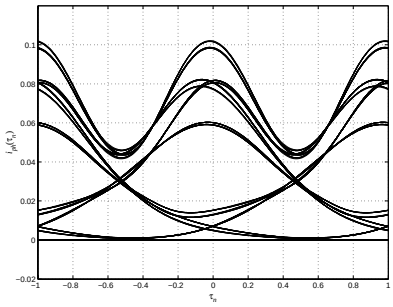

(f) AMI : $Q = 17.2$ dB

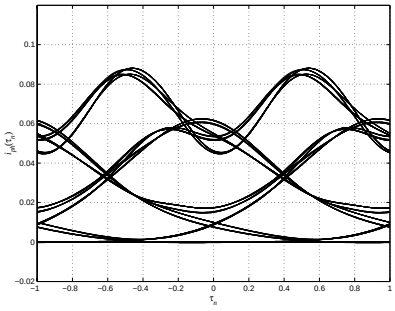

(g) No PM : $Q = 13.2$ dB

Fig. 6.4: Eye diagrams and corresponding Q at the receiver output when $z = 100$ km, $D = -0.5$ ps/(km·nm), $BW_{Tx} = 2$ and $P_{avg} = 6$ dBm (4 mW). Horizontal axis is normalized time τ_n, and vertical axis is $i_{ph}(\tau_n)$.

Table 6.1: Worst-case bit pattern when nearest neighboring bits are considered.

	APM	SaPM	SWM	CWSW	Duobinary	AMI	No PM
Bit 1	010	111	010	010	111	010	111
Bit 0	101	101	101	101	101	101	101

Table 6.2: Q in dB as a function of transmitter filter bandwidth BW_{Tx} when $z = 100$ km, $D = -0.5$ ps/(km·nm), and $P_{avg} = 6$ dBm (4 mW).

BW_{Tx}	1.0	1.5	2.0
APM	= No PM	17.8 ($B_{Opt} = 2.0$)	16.0 ($B_{Opt} = 1.2$)
SaPM	19.8 ($B_{Opt} = -1.4$)	18.4 ($B_{Opt} = -1.4$)	18.3 ($B_{Opt} = -1.2$)
SWM	18.0	17.9	17.6
CWSW	17.9	17.9	18.3
Duobinary	18.4	16.0	12.2
AMI	16.3	17.8	17.2
No PM	18.0	15.6	13.2

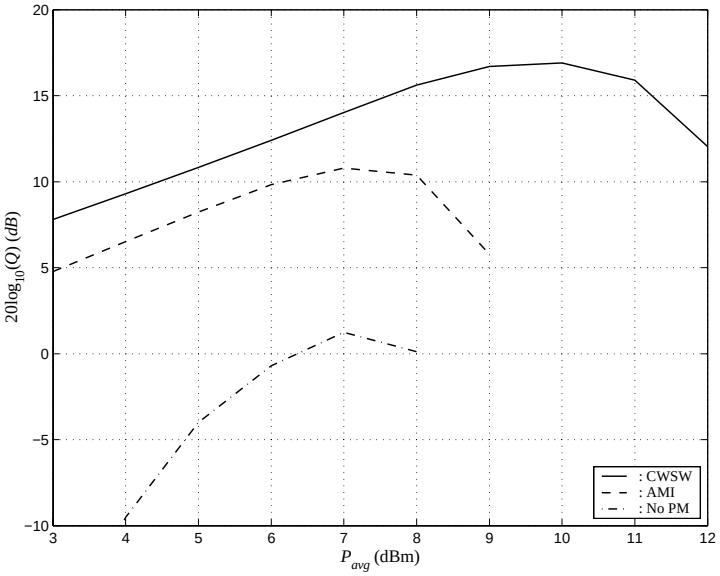

Fig. 6.5: System performance in terms of Q (dB) as a function of average transmitted power P_{avg} (dBm) when $D = +0.5$ ps/(km·nm), $BW_{Tx} = 4$, and $z = 190$ km.

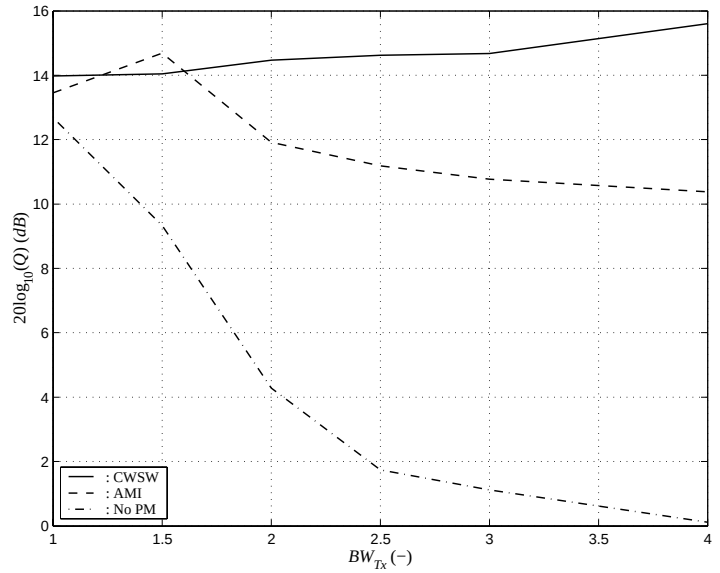

Fig. **6.6:** System performance in terms of Q (dB) as a function of normalized transmitter filter bandwidth BW_{Tx} when $D = +0.5$ ps/(km·nm), $P_{avg} = 8$ dBm, and $z = 190$ km

Table 6.3: Relationship between optimum system parameters and transmission distance z when $D = +0.5$ ps/(km·nm).

CWSW

z (km)	100	120	130	140	150	160	170	180	190	200
$P_{avg,Opt}$ (dBm)	10	10	10	10	10	10	10	10	10	10
BW_{Tx}	4	4	4	4	4	4	4	4	4	4
Q (dB)	38.6	34.1	31.8	29.4	26.8	24.1	21.8	19.4	16.9	14.3

AMI

z (km)	100	120	130	140	150	160	170	180	190	200
$P_{avg,Opt}$ (dBm)	8	8	8	8	8	8	8	8	8	8
BW_{Tx}	2	1.5	1.5	1.5	1.5	1.5	1.5	1.5	1.5	1.5
Q (dB)	37.3	32.4	30.1	27.8	25.5	23.1	20.4	17.6	14.7	11.6

No PM

z (km)	100	120	130	140	150	160	170	180	190	200
$P_{avg,Opt}$ (dBm)	10	9	9	9	9	9	9	9	8	8
BW_{Tx}	1.5	1.5	1.5	1.5	1.5	1.5	1.5	1.5	1	1
Q (dB)	36.2	31.0	28.5	26.0	23.5	20.9	18.6	15.4	12.7	10.1

Maximum Transmission Distance $z_{\max}$ for $Q = 15.6$ dB

	CWSW	AMI	No PM
$z_{\max}$ (km)	195	187	179
$P_{avg,Opt}$ (dBm)	10	8	9
BW_{Tx}	4	1.5	1.5

Table 6.4: Relationship between optimum system parameters and transmission distance z when $D = -0.5$ ps/(km·nm).

CWSW

z (km)	100	120	130	140	150	160	170	180	190	200
$P_{avg,Opt}$ (dBm)	10	9	9	8	8	7	7	–	–	–
BW_{Tx}	4	4	4	4	4	4	4	–	–	–
Q (dB)	35.4	29.4	26.3	23.2	19.9	16.5	12.9	–	–	–

AMI

z (km)	100	120	130	140	150	160	170	180	190	200
$P_{avg,Opt}$ (dBm)	11	9	8	7	7	6	5	–	–	–
BW_{Tx}	2	2	1.5	1.5	1.5	1.5	1	–	–	–
Q (dB)	33.6	27.3	24.4	21.4	18.4	15.4	12.8	–	–	–

No PM

z (km)	100	120	130	140	150	160	170	180	190	200
$P_{avg,Opt}$ (dBm)	12	7	7	7	6	6	6	–	–	–
BW_{Tx}	1.5	1	1	1	1	1	1	–	–	–
Q (dB)	31.9	26.6	23.9	21.3	18.6	15.8	13.1	–	–	–

Maximum Transmission Distance $z_{\max}$ for $Q = 15.6$ dB

	CWSW	AMI	No PM
$z_{\max}$ (km)	162	159	161
$P_{avg,Opt}$ (dBm)	7	6	6
BW_{Tx}	4	1.5	1

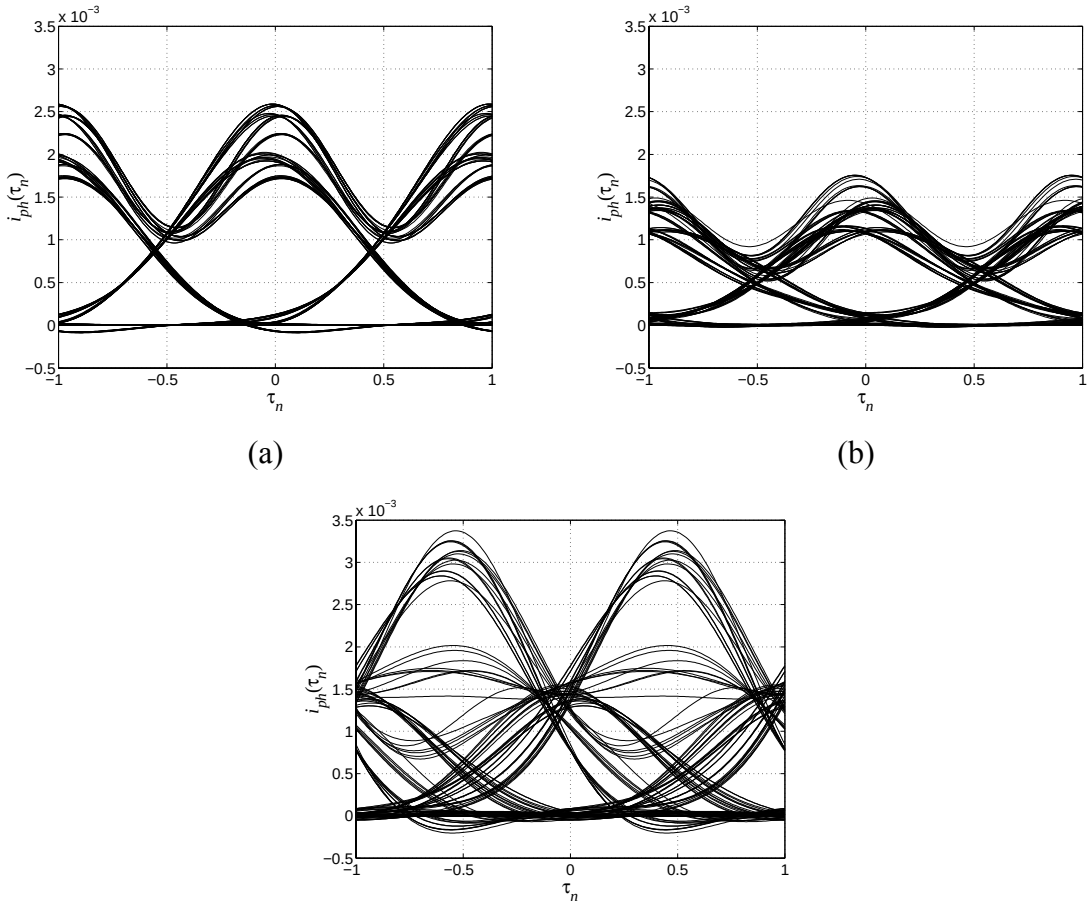

Fig. 6.7: Eye diagrams at optimum system parameters when $D = +0.5$ ps/(km·nm) and $z = 195$ km. (a) CWSW ($P_{avg,Opt} = 10$ dBm, $BW_{Tx} = 4$, $Q = 15.7$ dB), (b) AMI ($P_{avg,Opt} = 8$ dBm, $BW_{Tx} = 1.5$, $Q = 13.2$ dB), (c) No PM ($P_{avg,Opt} = 8$ dBm, $BW_{Tx} = 1$, $Q = 11.4$ dB).

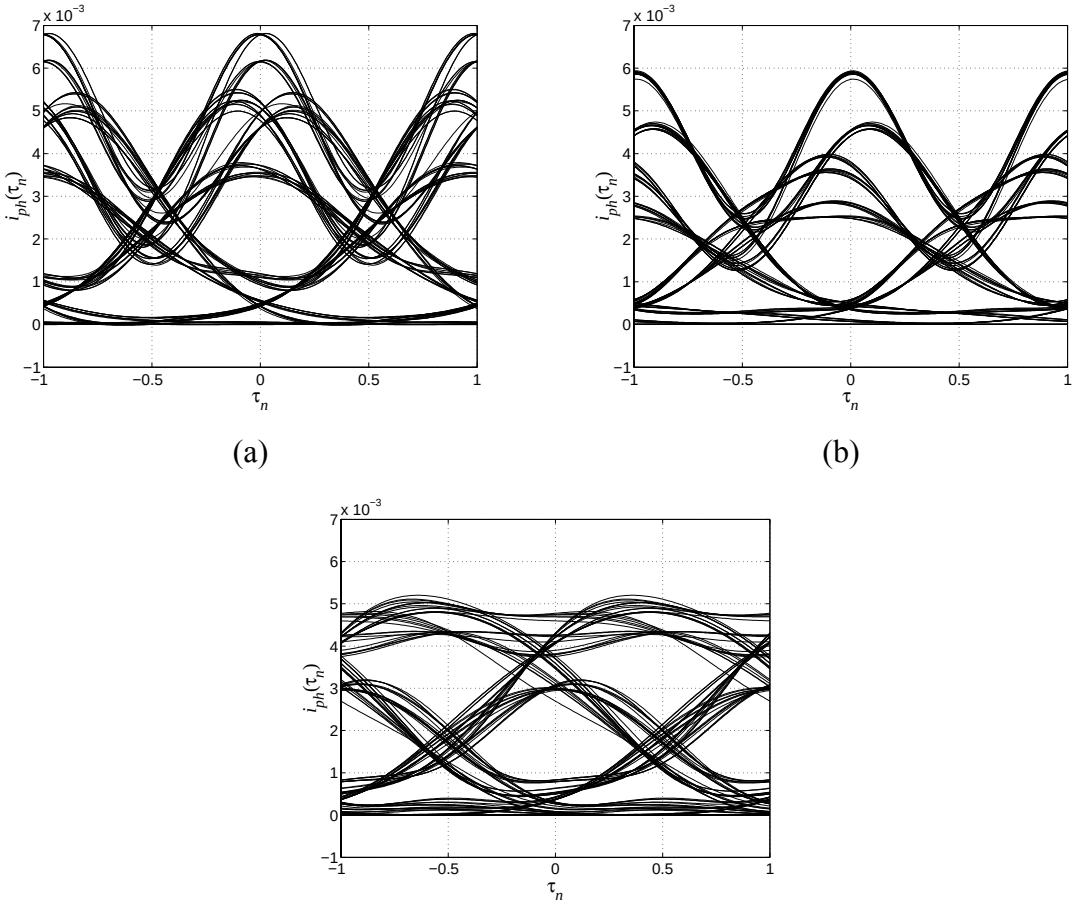

Fig. 6.8: Eye diagrams at optimum system parameters when $D = -0.5$ ps/(km·nm) and $z = 162$ km. (a) CWSW ($P_{avg,Opt} = 7$ dBm, $BW_{Tx} = 4$, $Q = 15.8$ dB), (b) AMI ($P_{avg,Opt} = 6$ dBm, $BW_{Tx} = 1.5$, $Q = 14.8$ dB), (c) No PM ($P_{avg,Opt} = 6$ dBm, $BW_{Tx} = 1$, $Q = 15.3$ dB).

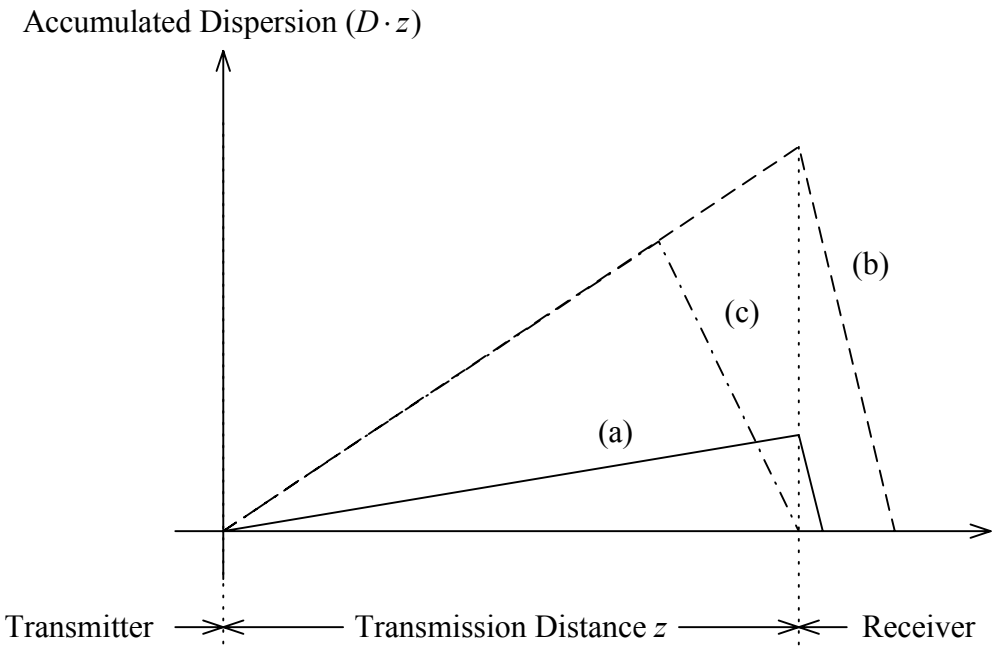

Fig. 6.9: Fiber configurations for single-span dispersion-managed systems. (a) Moderate local dispersion with modular dispersion compensating fiber at the receiver. (b) Large local dispersion with modular dispersion compensating fiber at the receiver. (c) Large local dispersion with dispersion compensating fiber employed as transmission fiber.

Table 6.5: Relationship between optimum system parameters and transmission distance z for systems employing TRSF and EHS-DK fiber.

CWSW

z (km)	20	60	100	120	130	140	150	160	170	180	190	200	210
$P_{avg,Opt}$ (dBm)	14	9	9	10	10	10	10	10	10	10	10	10	12
BW_{Tx}	1	1	1	1	1	1	1	1	1	1	1	1	1
Q (dB)	60.6	46.9	38.5	34.5	32.3	30.2	28.1	26.0	23.8	21.6	19.4	17.1	14.8

AMI

z (km)	20	60	100	120	130	140	150	160	170	180	190	200	210
$P_{avg,Opt}$ (dBm)	15	9	9	9	9	9	10	10	10	10	10	10	11
BW_{Tx}	2	4	4	4	4	4	4	4	4	4	4	4	4
Q (dB)	60.5	47.4	39.1	34.9	32.8	30.7	28.5	26.4	24.2	22.1	19.8	17.5	15.1

No PM

z (km)	20	60	100	120	130	140	150	160	170	180	190	200	210
$P_{avg,Opt}$ (dBm)	15	8	8	8	8	8	8	9	9	9	9	9	9
BW_{Tx}	2	4	4	4	4	4	4	4	4	4	4	4	4
Q (dB)	58.5	45.8	37.3	33.2	31.1	28.9	26.8	24.6	22.4	20.2	18.0	15.6	13.2

Length of EHS-DK Fiber

EHS-DK (km)	0.34	1.03	1.72	2.07	2.24	2.41	2.59	2.76	2.93	3.10	3.28	3.45	3.62

Maximum Transmission Distance $z_{\max}$ for $Q = 15.6$ dB

	CWSW	AMI	No PM
$z_{\max}$ (km)	206	208	200
$P_{avg,Opt}$ (dBm)	10	10	9
BW_{Tx}	1	4	4

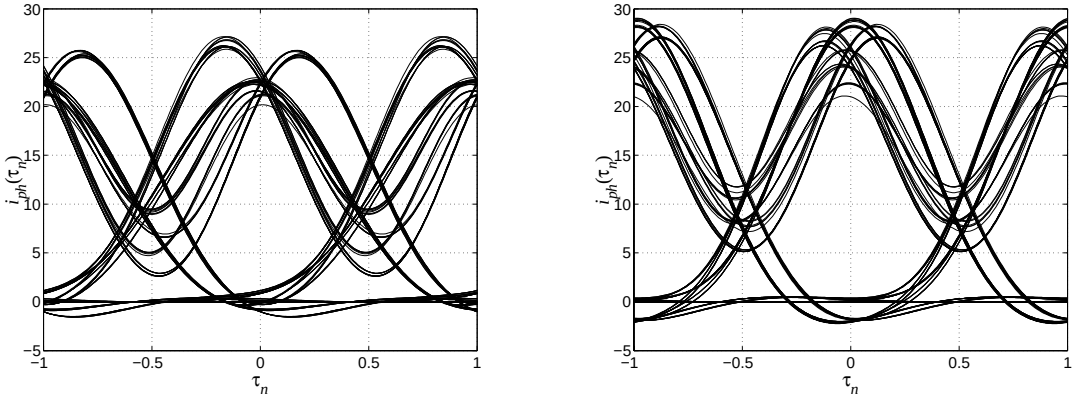

(a) (b)

Fig. 6.10: Eye diagrams in the case of AMI when $z = 20$ km and $P_{avg,Opt} = 15$ dBm. (a) $BW_{Tx} = 4$ ($Q = 59.3$ dB). (b) $BW_{Tx} = 2$ ($Q = 60.5$ dB).

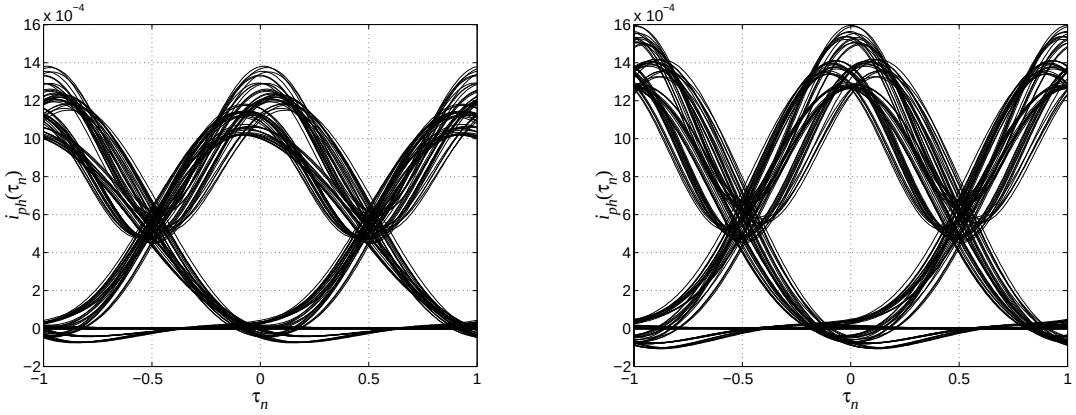

(a) (b)

Fig. 6.11: Eye diagrams in the case of CWSW when $z = 200$ km and $P_{avg,Opt} = 10$ dBm. (a) $BW_{Tx} = 4$ ($Q = 15.5$ dB). (b) $BW_{Tx} = 1$ ($Q = 17.1$ dB).

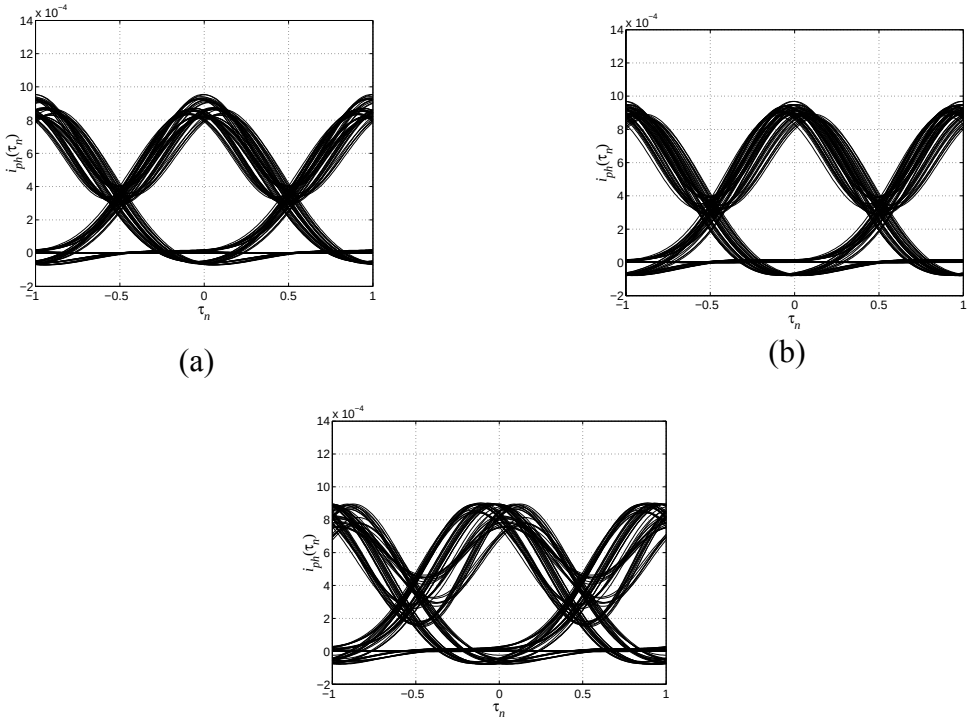

(a) (b)

(c)

Fig. 6.12: Eye diagrams at corresponding optimum BW_{Tx} when $z = 206$ km ($z_{\max}$ for CWSW) and $P_{avg} = 9$ dBm (optimum transmitted power for no PM). (a) CWSW ($BW_{Tx} = 1$, $Q = 15.5$ dB). (b) AMI ($BW_{Tx} = 4$, $Q = 15.8$ dB). (c) No PM ($BW_{Tx} = 4$, $Q = 14.2$ dB).

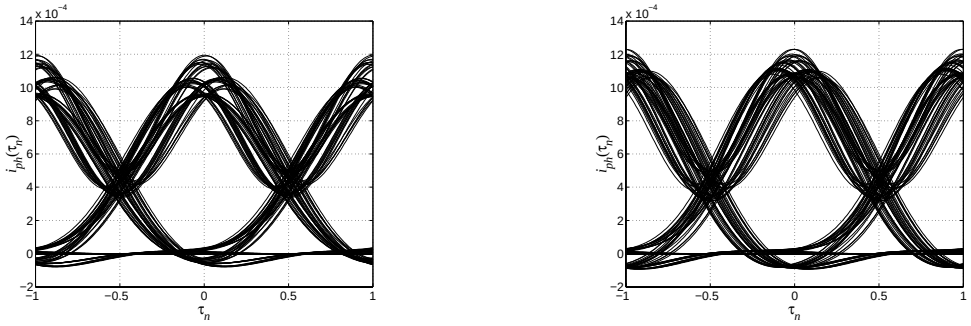

(a) (b)

Fig. 6.13: Eye diagrams at corresponding optimum system parameters when $z = 206$ km. (a) CWSW ($P_{avg,Opt} = 10$ dBm, $BW_{Tx} = 1$, $Q = 15.7$ dB), (b) AMI ($P_{avg} = 10$ dBm, $BW_{Tx} = 4$, $Q = 16.1$ dB).

Table 6.6: Relationship between optimum system parameters and transmission distance z for systems employing SSMF and EHS-DK fiber.

CWSW

z (km)	20	60	100	120	130	140	150	160	170	180	190	200
$P_{avg,Opt}$ (dBm)	13	10	10	8	11	11	11	11	11	11	11	11
BW_{Tx}	1	1	1	1	1	1	1	1	1	1	1	1
Q (dB)	58.1	46.6	37.0	30.8	29.9	27.4	24.9	22.3	19.7	17.0	14.1	11.0

AMI

z (km)	20	60	100	120	130	140	150	160	170	180	190	200
$P_{avg,Opt}$ (dBm)	13	12	13	13	13	13	13	13	13	13	13	13
BW_{Tx}	4	2	2	2	2	2	2	2	2	2	2	2
Q (dB)	58.5	47.5	38.1	32.4	30.7	28.2	25.7	23.2	20.7	18.1	15.3	12.5

No PM

z (km)	20	60	100	120	130	140	150	160	170	180	190	200
$P_{avg,Opt}$ (dBm)	13	10	10	8	11	11	11	11	11	11	11	11
BW_{Tx}	4	4	4	4	4	4	4	4	4	4	4	4
Q (dB)	57.5	45.5	35.9	29.8	28.7	26.2	23.7	21.1	18.5	15.8	12.9	9.9

Length of EHS-DK Fiber

EHS-DK (km)	1.47	4.40	7.33	8.79	9.53	10.26	11.00	11.72	12.46	13.19	13.92	14.66

Maximum Transmission Distance $z_{\max}$ for $Q = 15.6$ dB

	CWSW	AMI	No PM
$z_{\max}$ (km)	184	188	180
$P_{avg,Opt}$ (dBm)	11	13	11
BW_{Tx}	1	2	4

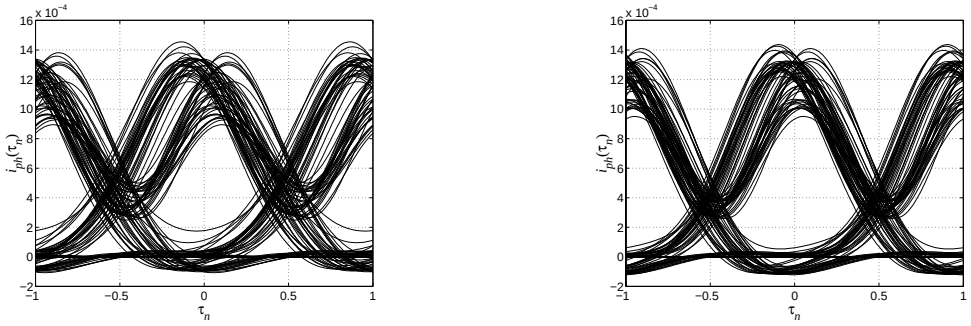

(a) (b)

Fig. 6.14: Eye diagrams for no PM when $z = 180$ km and $P_{avg,Opt} = 11$ dBm. (a) $BW_{Tx} = 2$ ($Q = 12.8$ dB). (b) $BW_{Tx} = 4$ ($Q = 15.8$ dB).

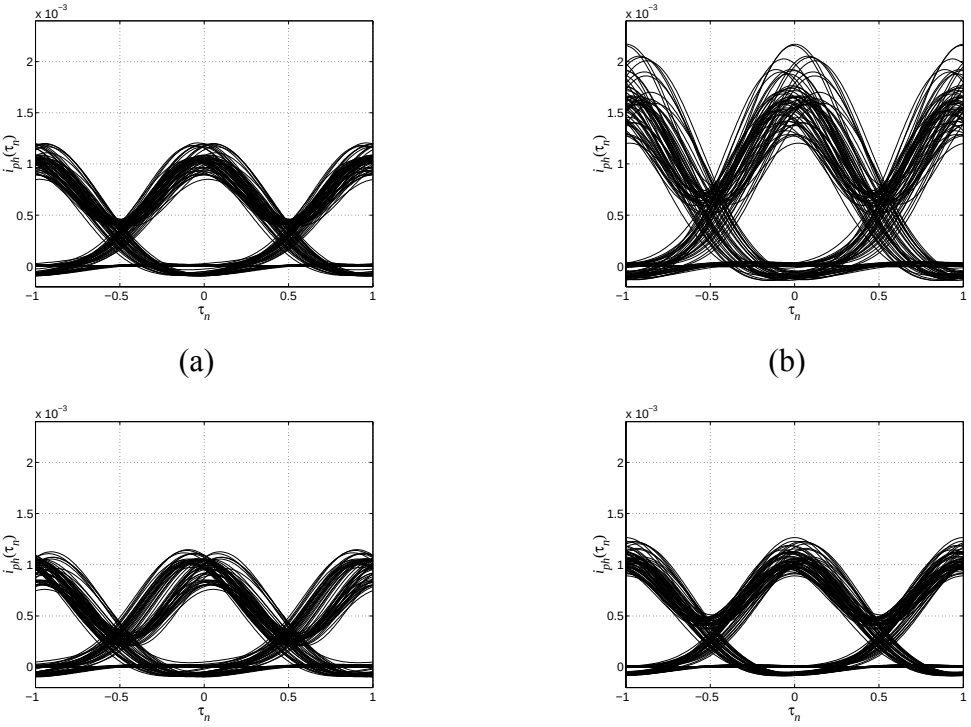

(a) (b)

(c) (d)

Fig. 6.15: Eye diagrams at corresponding optimum BW_{Tx} and $P_{avg,Opt}$ when $z = 184$ km ($z_{\max}$ for CWSW). (a) CWSW ($BW_{Tx} = 1$, $P_{avg,Opt} = 11$ dBm, $Q = 15.8$ dB). (b) AMI ($BW_{Tx} = 2$, $P_{avg,Opt} = 13$ dBm, $Q = 17.0$ dB).

(c) No PM ($BW_{Tx} = 4$, $P_{avg,Opt} = 11$ dBm, $Q = 14.6$ dB). (d) AMI ($BW_{Tx} = 2$, $P_{avg,Opt} = 11$ dBm, $Q = 16.3$ dB).

Table 6.7: Relationship between optimum system parameters and transmission distance z for systems employing SSMF and RDF.

CWSW

z (km)	20	60	100	120	130	140	150	160	170	180	190	200	210	220
$P_{avg,Opt}$ (dBm)	11	9	10	10	11	11	11	11	11	11	11	11	11	11
BW_{Tx}	1	1	1	1	1	1	1	1	1	1	1	1	1	1
Q (dB)	57.1	47.3	39.9	36.3	34.3	32.3	30.3	28.3	26.1	24.0	21.7	19.5	17.2	14.7

AMI

z (km)	20	60	100	120	130	140	150	160	170	180	190	200	210	220
$P_{avg,Opt}$ (dBm)	11	10	12	12	13	13	13	13	13	13	13	13	13	13
BW_{Tx}	4	2	2	2	2	2	2	2	2	2	2	2	2	2
Q (dB)	57.6	48.0	40.9	37.1	35.2	33.4	31.3	29.1	27.0	24.7	22.6	20.4	18.2	15.9

No PM

z (km)	20	60	100	120	130	140	150	160	170	180	190	200	210	220
$P_{avg,Opt}$ (dBm)	11	9	10	10	10	10	11	11	11	11	11	11	11	11
BW_{Tx}	4	4	4	4	4	4	4	4	4	4	4	4	4	4
Q (dB)	56.4	46.3	38.8	35.2	33.1	31.0	29.1	27.0	25.0	22.8	20.6	18.3	15.9	13.5

Length of SSMF

SSMF (km)	12.26	36.77	61.28	73.54	79.67	85.80	91.93	98.06	104.18	110.31	116.44	122.57	128.70	134.83

Length of RDF Fiber

RDF (km)	7.74	23.23	38.72	46.46	50.33	54.20	58.07	61.95	65.82	69.69	73.56	77.43	81.30	85.17

Maximum Transmission Distance $z_{\max}$ for $Q = 15.6$ dB

	CWSW	AMI	No PM
$z_{\max}$ (km)	216	221	211
$P_{avg,Opt}$ (dBm)	11	13	11
BW_{Tx}	1	2	4

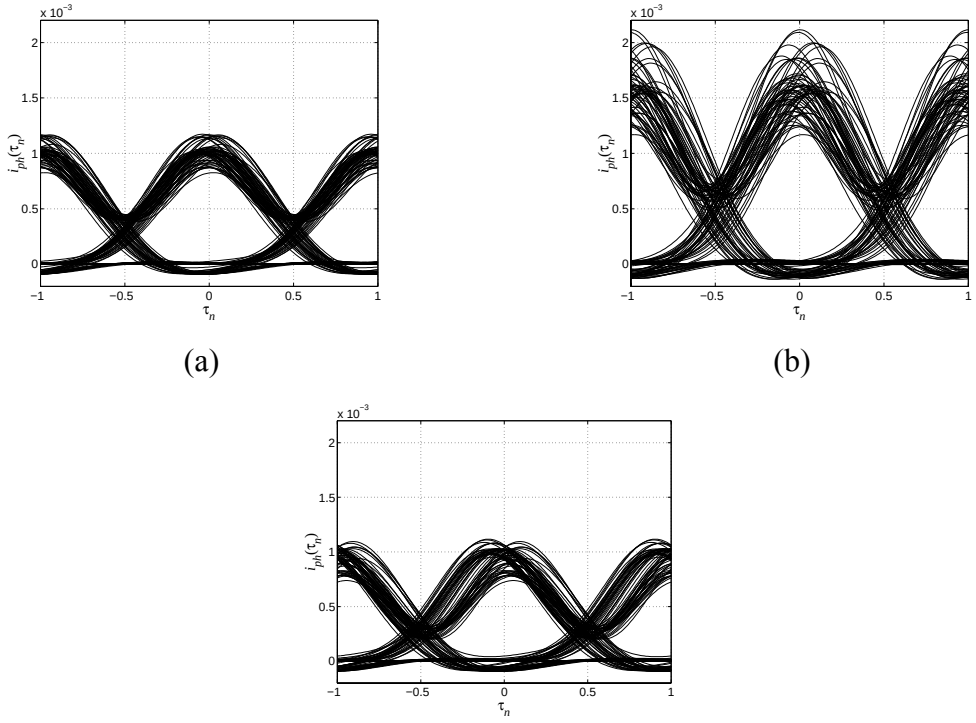

(a) (b)

(c)

Fig. 6.16: Eye diagrams at corresponding optimum BW_{Tx} and $P_{avg,Opt}$ when $z = 216$ km ($z_{\max}$ for CWSW). (a) CWSW ($BW_{Tx} = 1$, $P_{avg,Opt} = 11$ dBm, $Q = 15.7$ dB). (b) AMI ($BW_{Tx} = 2$, $P_{avg,Opt} = 13$ dBm, $Q = 16.8$ dB). (c) No PM ($BW_{Tx} = 4$, $P_{avg,Opt} = 11$ dBm, $Q = 14.5$ dB).

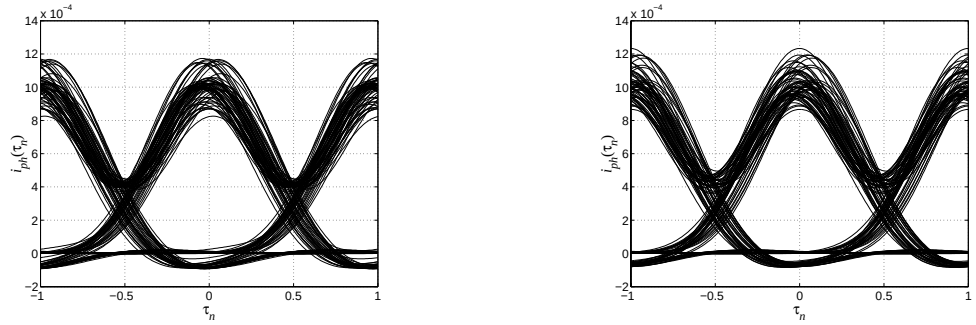

(a) (b)

Fig. 6.17: Eye diagrams for CWSW and AMI at corresponding optimum BW_{Tx} when $z = 216$ km ($z_{\max}$ for CWSW) and $P_{avg} = 11$ dBm. (a) CWSW ($BW_{Tx} = 1, Q = 15.7$ dB). (b) AMI ($BW_{Tx} = 2$, $Q = 16.2$ dB).

Table 6.8: Relationship between optimum system parameters and total number of spans for multiple-span dispersion-managed systems employing TRSF and EHS-DK fiber when the amplifier spacing (span length) is 160 km.

CWSW

Number of Spans	1	2	3	4
z (km)	160	320	480	640
$P_{avg,Opt}$ (dBm)	10	7	5	4
BW_{Tx}	1	1	1	1
Q (dB)	26.0	19.8	16.0	13.2

AMI

Number of Spans	1	2	3	4
z (km)	160	320	480	640
$P_{avg,Opt}$ (dBm)	10	7	6	5
BW_{Tx}	4	4	4	4
Q (dB)	26.4	20.3	16.5	13.6

No PM

Number of Spans	1	2	3	4
z (km)	160	320	480	640
$P_{avg,Opt}$ (dBm)	9	6	5	4
BW_{Tx}	4	4	4	4
Q (dB)	24.6	18.8	15.0	12.2

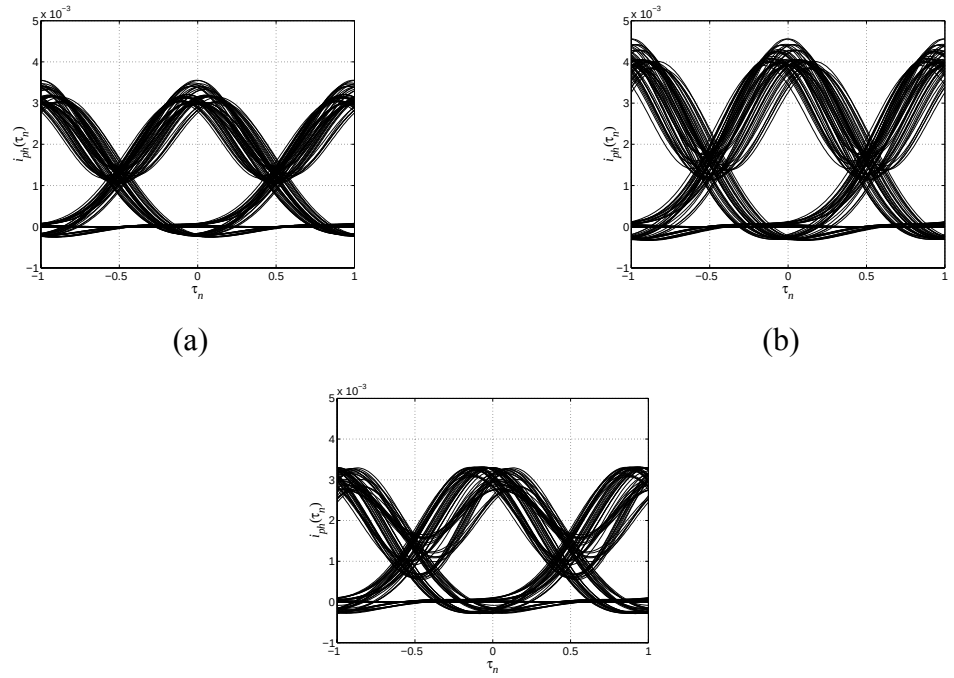

(a) (b)

(c)

Fig. 6.18: Eye diagrams at corresponding optimum system parameters listed in Table 6.8 when the total number of spans is 3 (total transmission distance of 480 km). (a) CWSW ($BW_{Tx}=1$, $P_{avg,Opt}=5$ dBm, $Q=16.0$ dB). (b) AMI ($BW_{Tx}=4$, $P_{avg,Opt}=6$ dBm, $Q=16.5$ dB). (c) No PM ($BW_{Tx}=4$, $P_{avg,Opt}=5$ dBm, $Q=15.0$ dB).

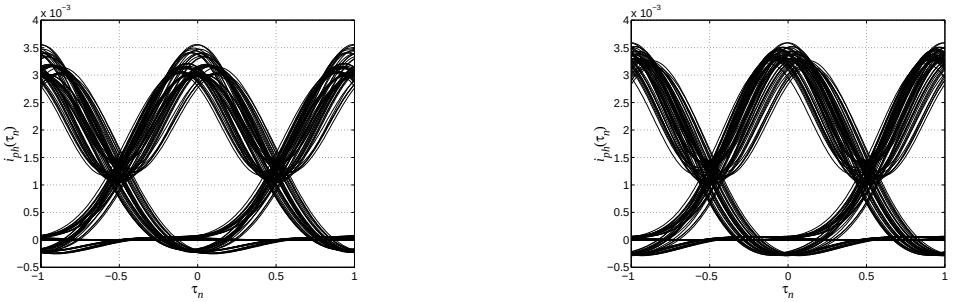

(a) (b)

Fig. 6.19: Eye diagrams for CWSW and AMI at corresponding optimum BW_{Tx} and $P_{avg,Opt}=5$ dBm (optimum for CWSW) when the total number of spans is 3 (total transmission distance of 480 km). (a) CWSW ($BW_{Tx}=1$, $Q=16.0$ dB). (b) AMI ($BW_{Tx}=4$, $Q=16.4$ dB).

Table 6.9: Relationship between optimum system parameters and total number of spans for multiple-span dispersion-managed systems employing TRSF and EHS-DK fiber when the amplifier spacing (span length) is 120 km.

CWSW

Number of Spans	1	2	3	4	5	6	7	8	9
z (km)	120	240	360	480	600	720	840	960	1080
$P_{avg,Opt}$ (dBm)	10	6	5	4	3	2	2	1	1
BW_{Tx}	1	1	1	1	1	1	1	1	1
Q (dB)	34.5	28.5	25.0	22.5	20.4	18.7	17.2	16.0	14.8

AMI

Number of Spans	1	2	3	4	5	6	7	8	9
z (km)	120	240	360	480	600	720	840	960	1080
$P_{avg,Opt}$ (dBm)	9	7	5	4	3	3	2	1	1
BW_{Tx}	4	4	4	4	4	4	4	4	4
Q (dB)	34.9	29.0	25.5	23.0	20.9	19.2	17.8	16.4	15.3

No PM

Number of Spans	1	2	3	4	5	6	7	8	9
z (km)	120	240	360	480	600	720	840	960	1080
$P_{avg,Opt}$ (dBm)	8	6	5	4	3	2	1	1	1
BW_{Tx}	4	4	4	4	4	4	4	4	4
Q (dB)	33.2	27.5	24.0	21.5	19.5	17.8	16.3	15.1	13.8

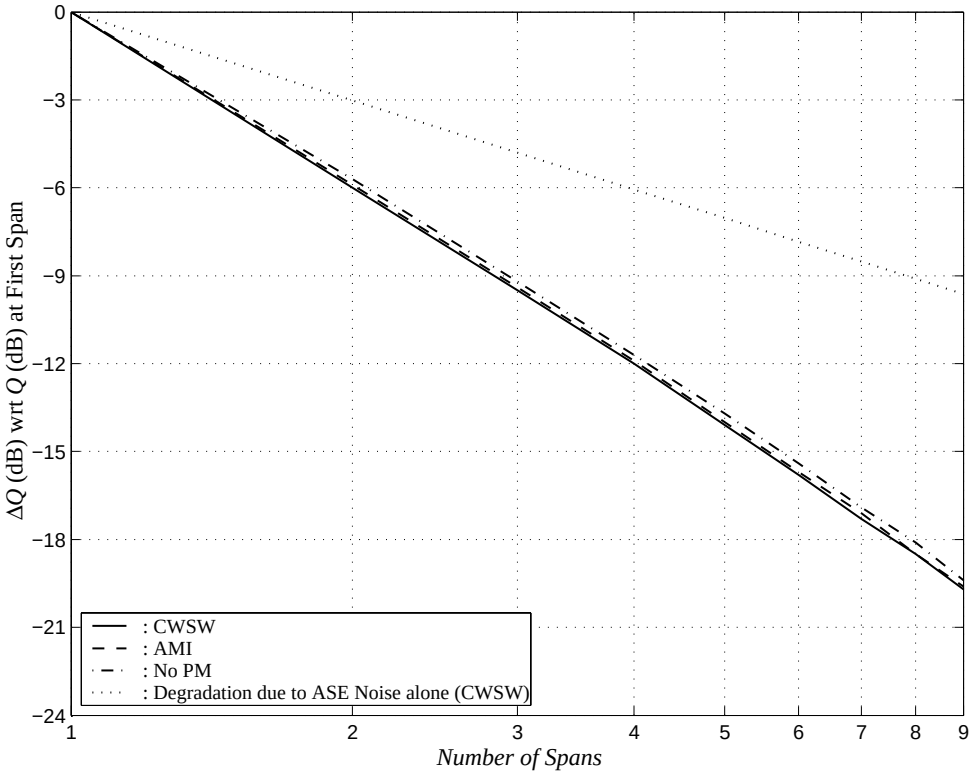

Fig. 6.20: Performance degradations in terms of Q, relative to the Q value at the first span, as a function of the number of spans when the amplifier spacing is 120 km for system employing TRSF and EHS-DK fiber.

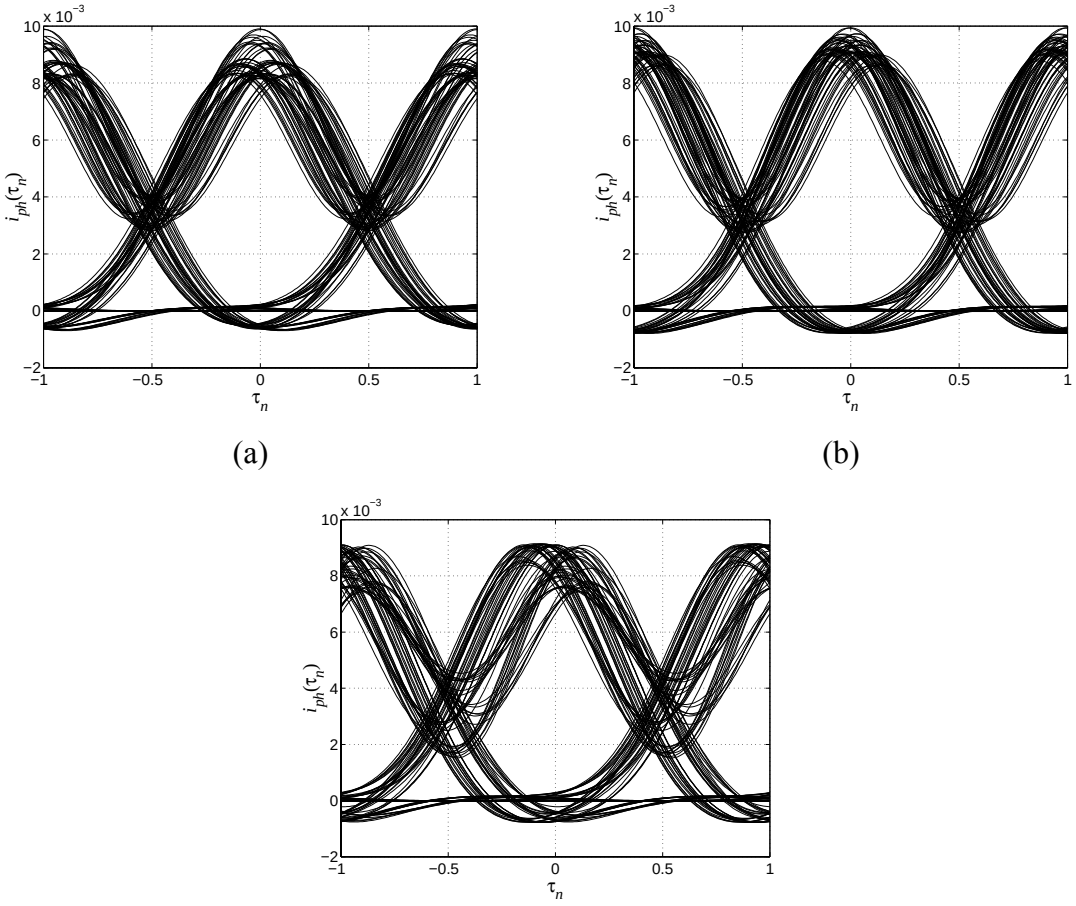

Fig. 6.21: Eye diagrams at corresponding optimum system parameters listed in Table 6.9 when the total number of spans is 8 (total transmission distance of 960 km). (a) CWSW ($BW_{Tx} = 1$, $P_{avg,Opt} = 1$ dBm, $Q = 16.0$ dB). (b) AMI ($BW_{Tx} = 4$, $P_{avg,Opt} = 1$ dBm, $Q = 16.4$ dB). (c) No PM ($BW_{Tx} = 4$, $P_{avg,Opt} = 1$ dBm, $Q = 15.1$ dB).

Table 6.10: Relationship between optimum system parameters and total number of spans for multiple-span dispersion-managed systems employing SSMF and RDF when the amplifier spacing (span length) is 160 km.

CWSW

Number of Spans	1	2	3	4
z (km)	160	320	480	640
$P_{avg,Opt}$ (dBm)	11	8	6	5
BW_{Tx}	1	1	1	1
Q (dB)	28.3	22.1	18.2	15.4

AMI

Number of Spans	1	2	3	4
z (km)	160	320	480	640
$P_{avg,Opt}$ (dBm)	13	10	9	8
BW_{Tx}	2	2	2	2
Q (dB)	29.1	23.2	19.6	16.9

No PM

Number of Spans	1	2	3	4
z (km)	160	320	480	640
$P_{avg,Opt}$ (dBm)	11	8	6	5
BW_{Tx}	4	4	4	4
Q (dB)	27.0	21.1	17.3	14.4

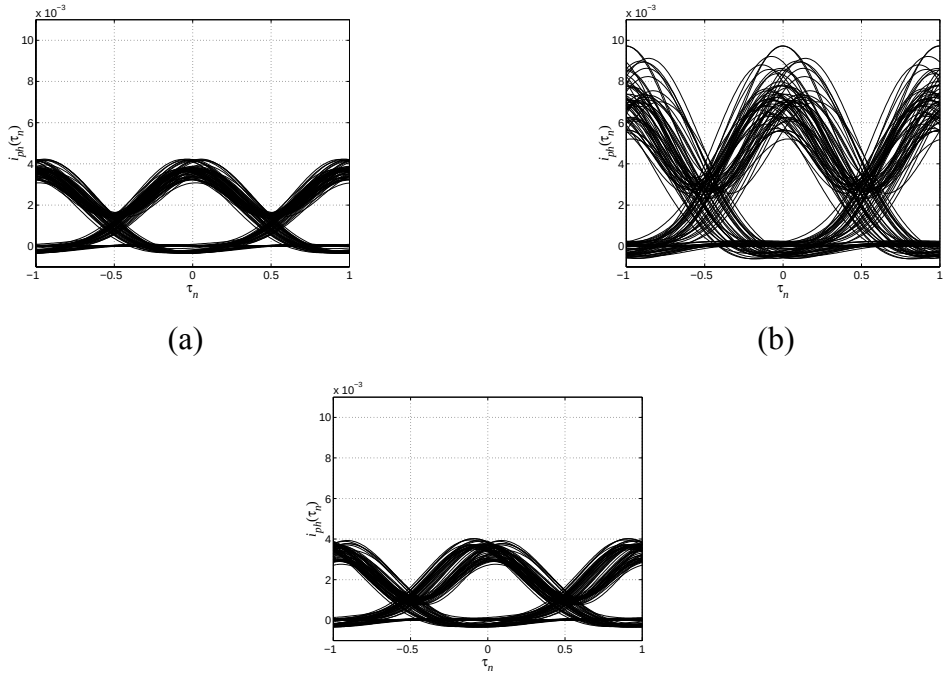

(a) (b)

(c)

Fig. 6.22: Eye diagrams at corresponding optimum system parameters listed in Table 6.9 when the total number of spans is 4 (640 km of total transmission distance). (a) CWSW ($BW_{Tx} = 1$, $P_{avg,Opt} = 5$ dBm, $Q = 15.4$ dB). (b) AMI ($BW_{Tx} = 2$, $P_{avg,Opt} = 8$ dBm, $Q = 16.9$ dB). (c) No PM ($BW_{Tx} = 4$, $P_{avg,Opt} = 5$ dBm, $Q = 14.4$ dB).

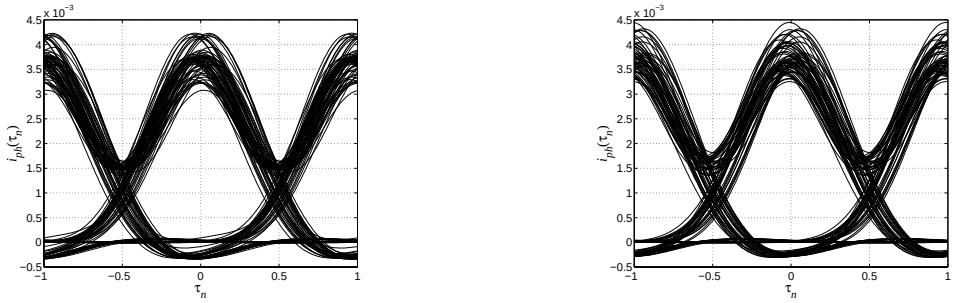

(a) (b)

Fig. 6.23: Eye diagrams for CWSW and AMI at corresponding optimum BW_{Tx} and $P_{avg,Opt} = 5$ dBm (optimum for CWSW) when the total number of spans is 4 (640 km of total transmission distance). (a) CWSW ($BW_{Tx} = 1$, $Q = 15.4$ dB). (b) AMI ($BW_{Tx} = 2$, $Q = 16.0$ dB).

Table 6.11: Relationship between optimum system parameters and total number of spans for multiple-span dispersion-managed systems employing SSMF and RDF when the amplifier spacing (span length) is 120 km.

CWSW

Number of Spans	1	2	3	4	5	6	7	8	9	10	11	12
z (km)	120	240	360	480	600	720	840	960	1080	1200	1320	1440
$P_{avg,Opt}$ (dBm)	10	7	6	4	4	3	2	2	1	1	0	0
BW_{Tx}	1	1	1	1	1	1	1	1	1	1	1	1
Q (dB)	36.3	30.3	26.7	24.1	22.0	20.4	18.9	17.6	16.4	15.3	14.4	13.5

AMI

Number of Spans	1	2	3	4	5	6	7	8	9	10	11	12
z (km)	120	240	360	480	600	720	840	960	1080	1200	1320	1440
$P_{avg,Opt}$ (dBm)	12	10	8	7	6	5	5	4	4	3	3	3
BW_{Tx}	2	2	2	2	2	2	2	2	2	2	2	2
Q (dB)	37.1	31.3	27.8	25.3	23.3	21.7	20.3	19.0	17.9	16.9	16.0	15.1

No PM

Number of Spans	1	2	3	4	5	6	7	8	9	10	11	12
z (km)	120	240	360	480	600	720	840	960	1080	1200	1320	1440
$P_{avg,Opt}$ (dBm)	10	7	6	4	3	3	2	1	1	1	0	0
BW_{Tx}	4	4	4	4	4	4	4	4	4	4	4	4
Q (dB)	35.2	29.3	25.7	23.1	21.1	19.4	17.9	16.5	15.4	14.3	13.3	12.4

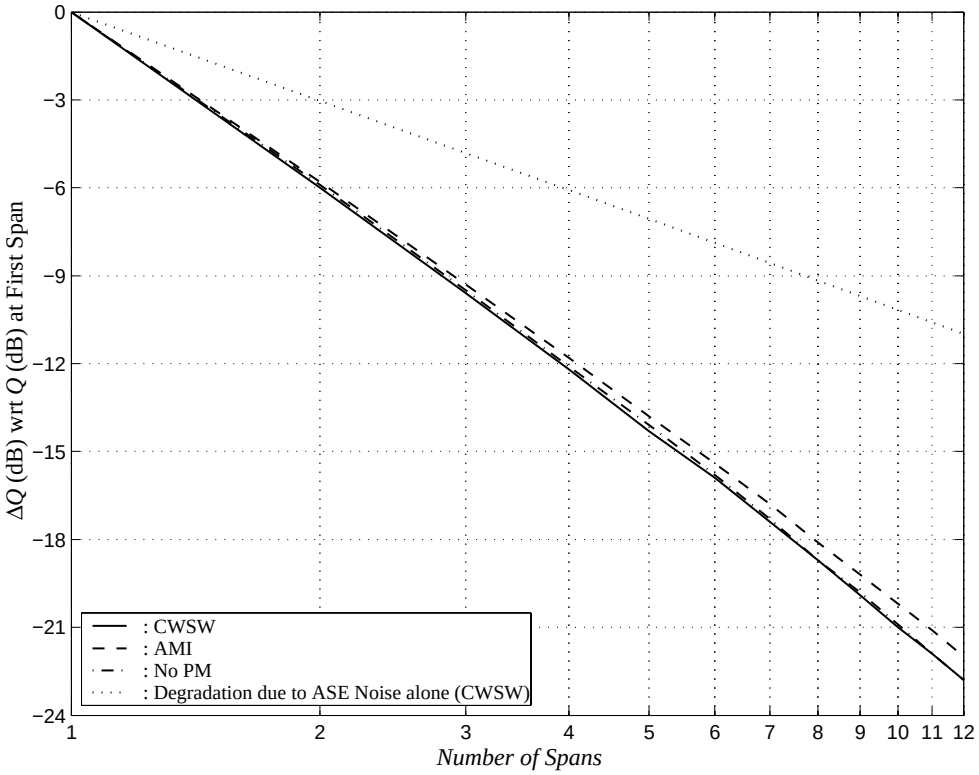

Fig. 6.24: Performance degradations in terms of Q, relative to the Q value at the first span, as a function of the number of spans when the amplifier spacing is 120 km for system employing SSMF and RDF.

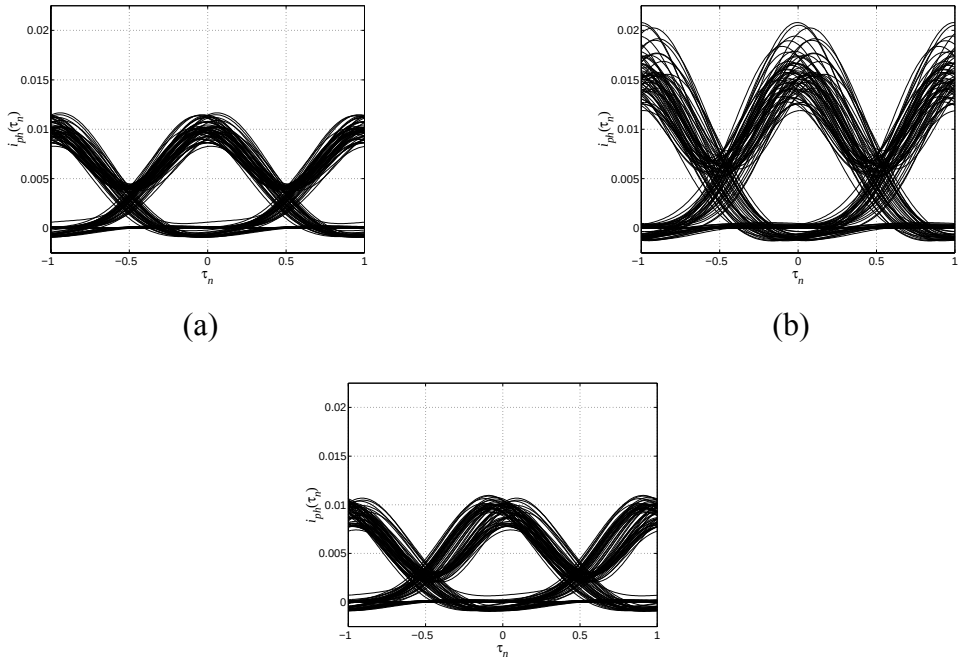

(a) (b)

(c)

Fig. 6.25: Eye diagrams at corresponding optimum system parameters listed in Table 6.10 when the total number of spans is 10 (1200 km of total transmission distance). (a) CWSW ($BW_{Tx}=1$, $P_{avg,Opt}=1$ dBm, $Q=15.3$ dB). (b) AMI ($BW_{Tx}=2$, $P_{avg,Opt}=3$ dBm, $Q=16.9$ dB). (c) No PM ($BW_{Tx}=4$, $P_{avg,Opt}=1$ dBm, $Q=14.3$ dB).

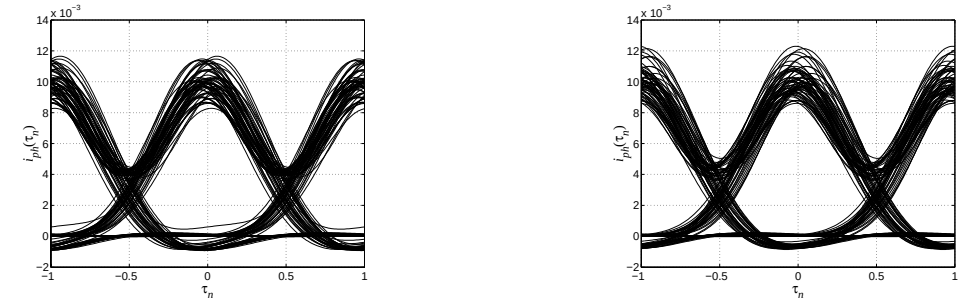

(a) (b)

Fig. 6.26: Eye diagrams for CWSW and AMI at corresponding optimum BW_{Tx} and $P_{avg,Opt}=1$ dBm (optimum for CWSW) when the total number of spans is 10 (1200 km of total transmission distance). (a) CWSW ($BW_{Tx}=1$, $Q=15.3$ dB). (b) AMI ($BW_{Tx}=2$, $Q=16.1$ dB).

Table. 6.12: Relationship between system performance in terms of Q and multiplexer filter bandwidth BW_{Mux} for single-span system employing TRSF and EHS-DK fiber in the case of CWSW signal format when the transmission distance is 200 km and $BW_{Tx}=1$. Note that without the multiplexer filter at the fiber input $Q=17.1$ dB at $P_{avg,Opt}=10$ dBm and $BW_{Tx}=1$.

BW_{Mux}	1	1.5	2	2.5	3	4
$P_{avg,Opt}$ (dBm)	9	10	10	10	10	10
Q (dB)	10.4	14.7	16.3	17.1	17.1	17.1

Table. 6.13: Relationship between system performance in terms of Q and multiplexer filter bandwidth BW_{Mux} for single-span system employing SSMF and RDF in the case of CWSW signal format when the transmission distance is 210 km and $BW_{Tx}=1$. Note that without the filter at the fiber input $Q=17.2$ dB at $P_{avg,Opt}=11$ dBm and $BW_{Tx}=1$.

BW_{Mux}	1	1.5	2	2.5	3	4
$P_{avg,Opt}$ (dBm)	10	11	11	11	11	11
Q (dB)	10.7	16.0	17.4	17.2	17.2	17.2

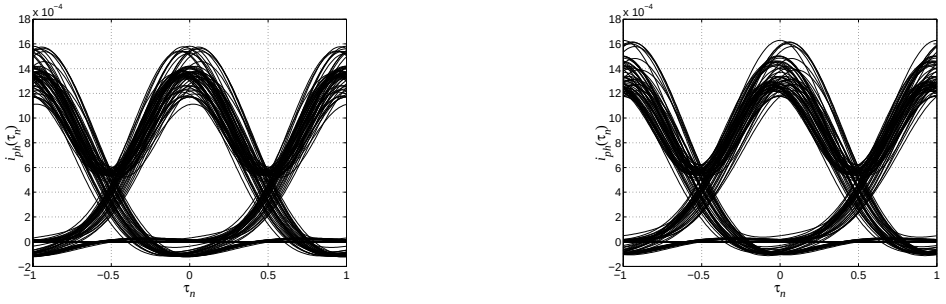

(a) (b)

Fig. 6.27: Eye diagrams for CWSW when $z=210$ km, $BW_{Tx}=1$, and $P_{avg,Opt}=11$ dBm. (a) $BW_{Mux}=2$. (b) $BW_{Mux}=4$.